Modeling demographic-driven vegetation dynamics and ecosystem biogeochemical cycling in NASA GISS's Earth system model (ModelE-BiomeE v.1.0)

Ensheng Weng[1,2], Igor Aleinov[1,2], Ram Singh[1,2], Michael J. Puma[1,2], Sonali S. McDermid[3], Nancy Y. Kiang[2], Maxwell Kelley[2], Kevin Wilcox[4], Ray Dybzinski[5], Caroline E. Farrior[6], Stephen W. Pacala[7], Benjamin I. Cook[2]

[1]Center for Climate Systems Research, Columbia University, New York, NY 10025, USA

[2]NASA Goddard Institute for Space Studies, 2880 Broadway, New York, NY 10025, USA

[3]Department of Environmental Studies, New York University, New York, NY 10003, USA

[4]Department of Ecosystem Science and Management, University of Wyoming, Laramie, WY 82071, USA

[5]Institute of Environmental Sustainability, Loyola University Chicago, Chicago, IL 60660, USA

[6]Department of Integrative Biology, University of Texas at Austin, Austin, TX 78712, USA

[7]Department of Ecology & Evolutionary Biology, Princeton University, Princeton, NJ 08544, USA

Corresponding author: Ensheng Weng (wengensheng@gmail.com; phone: 212-678-5585)

Submitted to **Geoscientific Model Development**

Abstract: We developed a new demographic vegetation model, BiomeE, to improve the representation of vegetation demographic dynamics and ecosystem biogeochemical cycles in the NASA Goddard Institute of Space Studies' ModelE Earth system model. This model includes the processes of plant growth, mortality, reproduction, vegetation structural dynamics, and soil carbon and nitrogen storage and transformations. The model combines the plant physiological processes of ModelE's original vegetation model, Ent, with minor adaptations to fit the new allometry and vegetation structure with the plant demographic and ecosystem nitrogen processes represented in the Geophysical Fluid Dynamics Laboratory's LM3-PPA. For global applications, we added a new set of plant functional types to represent global vegetation functional diversity, including trees, shrubs, and grasses, and a new phenology model to deal with seasonal changes in temperature and soil water availability. Competition for light and soil resources is individual-based, which makes the modeling of transient compositional changes and vegetation succession possible. BiomeE will allow ModelE to simulate long-term biogeophysical and biogeochemical feedbacks between the climate system and land ecosystems. BiomeE simulates, with fidelity comparable to other models, the dynamics of vegetation and soil biogeochemistry, including leaf area index, vegetation structure (e.g., height, tree density, size distribution, crown organization), and ecosystem carbon and nitrogen storage and fluxes. Further, BiomeE also allows for the simulations of transient vegetation dynamics and eco-evolutionary optimal community assemblage in response to past and future climate changes by incorporating core ecological processes, including demography, competition, and community assembly.

Key words: Biogeochemical cycles, Eco-evolutionary optimality, Ecosystem modeling, Plant traits, Vegetation dynamics

Deleted: from

Deleted:

1 Introduction

Terrestrial ecosystems play a critical role in climate systems by regulating exchanges of energy, moisture, and carbon dioxide between the land surface and the atmosphere (Sellers, 1997; Pielke et al., 1998; Meir et al., 2006). In turn, climate change has significantly affected vegetation photosynthesis, water use efficiency, mortality, regeneration, and structure through gradual changes in temperature and atmospheric CO_2 concentration ($[CO_2]$) together with shifts in climate extremes (Keenan et al., 2013; Huang et al., 2015; Brando et al., 2019; McDowell et al., 2020). These responses have triggered structural and compositional shifts in global vegetation. For example, global forest mortality has increased in recent years (Allen et al., 2010; Anderegg et al., 2012), tree sizes have decreased (Zhou et al., 2014; McDowell et al., 2020), and species composition has shifted to more opportunistic species (Clark et al., 2016; Brodribb et al., 2020). The shifts in vegetation function, composition, and structure can change the boundary conditions of the land surface and affect the climate system (Nobre et al., 1991; Avissar and Werth, 2005; Garcia et al., 2016; Green et al., 2017; Zeng et al., 2017). Realistic simulation of these processes is therefore critical for Earth system models (ESMs).

The vegetation dynamics in ESMs are usually simulated using dynamic global vegetation models (DGVMs) (Prentice et al., 2007), most of which are simplified in their representation of ecological processes. The core assumptions of many vegetation models are a big-leaf canopy, vegetation represented by only a few plant functional types (PFTs), single cohort-based vegetation dynamics ("single-cohort" assumption, where the vegetation community at a land unit are simulated as a collection of identical plants), lumped-pool-based biogeochemical cycles and first order decay of soil organic matter. The competition of plant individuals and vegetation types is approximately simulated as a function of productivity or Lotka-Volterra equations to predict

Deleted: the

Deleted: vegetation

fractional PFT coverage (e.g., SDVGM, HYBRID, TRIFFID) (Friend et al., 1997; Woodward et al., 1998; Sitch et al., 2003). These simplifying assumptions make it possible to simulate the complex interactions of biological and ecological processes at the global scale.

These models are generally successful in reproducing land surface carbon, energy, and water fluxes after extensive tuning against data from sites, observational networks, and satellite remote sensing. However, the uncertainty of model predictions is high, and predictions can diverge substantially across different models (Friedlingstein et al., 2014; Arora et al., 2020). Lack of functional diversity and community assembly processes is one of the key issues in the vegetation modeling of ESMs, which makes the models unable to predict transient dynamics of vegetation composition and structure. A more mechanistic design that uses the fundamental principles of ecology to simulate the emergent properties of ecosystems for predicting ecosystem dynamics may therefore be necessary (Scheiter et al., 2013; Weng et al., 2017).

To this end, extensive efforts have been made to improve the representation of transient vegetation dynamics based on ecological theories and conceptual models. Two pivotal advances have been made in ecological vegetation modeling: 1) Demographic processes and trait-based representation of processes have been developed to improve the representation of functional diversity and size (Pavlick et al., 2013; Fisher et al., 2015; Weng et al., 2015; Argles et al., 2020) and 2) eco-evolutionary optimal and game theoretical approaches have been proposed to predict the flexibility of parameters and processes (McNickle et al., 2016; Weng et al., 2017). These concepts are mainly applied in modeling photosynthesis (Prentice et al., 2014; Wang et al., 2017), allocation (Farrior et al., 2013; Dybzinski et al., 2015), and evolutionarily stable strategy of plant traits (Falster et al., 2017; Weng et al., 2017). These ideas for incorporating ecological

and evolutionary principles into ESMs have been summarized in several recent review papers (Franklin et al., 2020; Harrison et al., 2021; Kyker-Snowman et al., 2022).

There are still major challenges to integrating the more sophisticated ecological modeling approaches into land models, which explicitly simulate energy, water, and carbon fluxes at high frequency time steps for interacting with the atmosphere and climate systems. The details of vegetation dynamics, including leaf photosynthesis, respiration, plant growth, demographic processes, community assembly, vegetation structure, and competition output, must be well-organized hierarchically and computed efficiently (Fisher and Koven, 2020; Franklin et al., 2020). Representing these processes in ESMs, however, can complicate model structure and behavior, especially the interaction between physiology and vegetation composition, and cause large increases in the computational burden. Thus, the implementation of detailed vegetation demographic processes and population dynamics into ESMs would benefit from more parsimonious approaches.

Including highly complex processes does not necessarily increase model predictive skills (Forster, 2017; Hourdin et al., 2017; Famiglietti et al., 2021). On the contrary, it may greatly obscure model transparency and increase uncertainty; positive feedbacks in these processes may result in large and unanticipated shifts of vegetation states. Any small differences in model settings or parameters can result in distinct predictions, especially for vegetation structure, which is supposed to be predicted by these types of models. These processes make demographic vegetation models often unreliable when compared to the well-tuned "single-cohort" vegetation models that simplify the reproduction and mortality as growth and turnover of continuous biomass pools. Additionally, the long history of land models and the requirements of backward compatibility (i.e., reversing the model to its previous versions) mean developers must often

Deleted: se

Deleted: the complex

Deleted: of ESMs

Deleted: where the

Deleted: ions

Deleted: of

Deleted: ies are required

Deleted: the key functions from

Deleted: biogeochemical fluxes between pools

Deleted: for

Deleted: size categories

Deleted: , and

Deleted: even

Deleted: differences

Deleted: in

Deleted: functions

build their new functions on top of previous modeling assumptions and coding structure (Fisher and Koven, 2020), adding up to multiple adjustments of previous processes and making the model untraceable.

To explicitly model the transient dynamics of ecosystems in ESMs while preserving model traceability, we need clear assumptions, detailed physical processes, and traceable model structure. For the best chance of accurate predictions outside of the model's testing data, model processes should be based on the fundamental biological and ecological principles to predict ecosystem emergent properties, instead of fitting the emergent patterns directly as many models do currently. To achieve this, we need to properly represent the tradeoffs of plant traits, balance the complexity of the model structure and priority for the processes that are required by the general circulation models (GCM), and also make model assumptions transparent and processes robust. These requirements make it difficult to fully implement the modeling approaches that are well-developed in the ecological modeling community (e.g., Falster et al., 2016; Berzaghi et al., 2019; Weiskopf et al., 2022).

This paper describes a vegetation demographic and soil organic decomposition model that is incorporated into the NASA Goddard Institute for Space Studies (GISS) Earth system model, ModelE (Kelley et al., 2020). Our goal is to develop a parsimonious and transparent terrestrial ecosystem model that 1) allows ModelE to simulate the ecological dynamics of terrestrial ecosystems and vegetation at the global scale and 2) sets up a modeling framework for solving some of the major challenges for incorporating important ecological mechanisms into ESMs. For (1), we have incorporated the core ecosystem processes, including plant growth, demography, community assembly, and ecosystem carbon and nitrogen cycles. For (2), we have defined a set of PFTs that are plant trait-based and a competition scheme that is individual-based. In this

Deleted: developed

paper, we describe this model in detail, and evaluate its performance compared to both observations and other state-of-the-art DGVMs.

2 Model Description

2.1 GISS ModelE and BiomeE overview

ModelE has a land model for representing land surface hydrology (TerraE) (Rosenzweig and Abramopoulos, 1997; Schmidt et al., 2014) and a vegetation biophysics scheme (from the Ent Terrestrial Biosphere Model; TBM) (Kim et al., 2015; Ito et al., 2020; Kelley et al., 2020), with fixed vegetation traits (e.g., leaf mass per area, C:N ratio), fixed biomass, canopy height, and plant density, and seasonal leaf area index prescribed from a satellite-derived data set (Ito et al., 2020). The Ent TBM calculates canopy radiative transfer (Friend & Kiang 2005), canopy albedo, canopy conductance, photosynthesis, autotrophic respiration, and phenological behaviors (Kim et al., 2015). The carbon allocation scheme of Kim et al. (2015) is used in ModelE with prescribed canopy structure and leaf area index (LAI), routing the carbon that would otherwise be allocated to plant tissues via growth instead directly as litter into soil carbon pools, thus conserving carbon for fully coupled carbon cycle simulations, but resulting possibly in imbalanced plant carbon reserve pools where the prescribed canopy structure is not in equilibrium with the simulated climate (Ito et al., 2020).

The Biome Ecological strategy simulator (BiomeE) is derived from Geophysical Fluid Dynamics Laboratory's vegetation model, LM3-PPA (Weng et al., 2015, 2017, 2019). It simulates plant physiology, vegetation demography, adaptive dynamics (eco-evolutionary adaptation), and ecosystem carbon, nitrogen, and water cycles (Figure 1). In this model, the PFTs are defined by a set of combined plant traits with their values sampled from the observed ranges to represent a

Deleted: some

Deleted: of leaf biophysics

Deleted: Fig.

specific plant type. Individual plants are categorized into cohorts and arranged in different vertical canopy layers according to their height and crown area following the rules of the Perfect Plasticity Approximation model (PPA, Strigul et al., 2008). Sunlight is partitioned into canopy crown layers according to Beer's law (Beer, 1852; Swinehart, 1962). The cohort is the basic unit to carry out physiological and demographic activities, e.g., photosynthesis, respiration, growth, reproduction, mortality, and competition with other individuals.

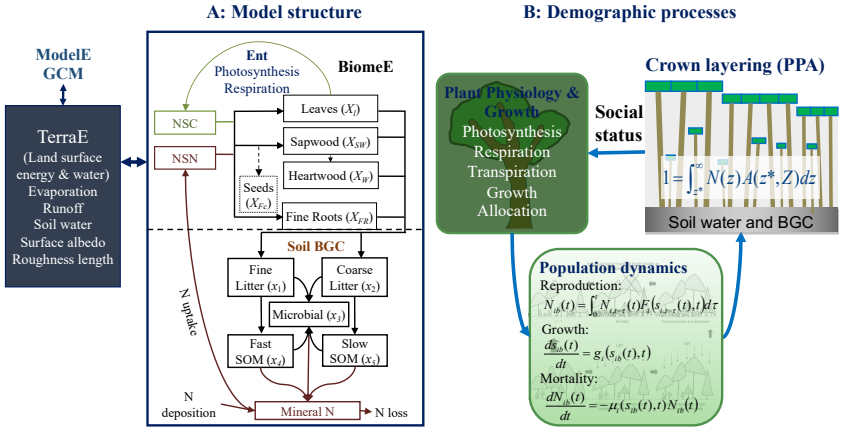

Figure 1 Schematic diagram of the coupling of BiomeE into ModelE

Panel A shows the structure of carbon and nitrogen pools and fluxes, and the interactions of BiomeE with TerraE, the land surface model in ModelE. The lines are the flows of carbon (green), nitrogen (brown), and coupled carbon and nitrogen (black). The green box is for carbon only. The brown boxes are N pools. The black boxes are for both carbon and nitrogen pools. The C:N ratios of leaves, wood, fine roots, and microbes are fixed and those of liters and SOM pools are dynamic with input and output. Panel b shows the demographic processes of BiomeE and the key processes of population dynamics.

The demographic processes generate and remove cohorts and change the size and density of plant individuals in the cohorts. With explicit description of cohort size, organization, and

composition during a model run, the model simulates competition for light and soil resources, community assembly and vegetation structural dynamics. These processes are hierarchically organized in this model and run at various time steps: half-hourly or hourly for plant physiology and soil organic matter decomposition, daily for growth and phenology, and yearly for demography.

We coupled the BiomeE model into ModelE's land model for simulating global dynamics of vegetation and biogeochemical cycles and their feedback to the climate system. For extending this model to the global scale, we designed a new set of PFTs to represent the functional diversity of global vegetation and a new phenological scheme to deal with temperature and water seasonality. Leaf photosynthesis processes are taken from ModelE's existing vegetation model, Ent (Kim et al., 2015), and used to calculate the carbon budget that drives vegetation dynamics. Plant growth and demographic processes and the soil organic matter decomposition and nitrogen cycle processes are from BiomeE (Figure 1). The land surface energy and water fluxes are calculated by TerraE with land surface characteristics jointly defined by the vegetation model.

Deleted: standalone

Deleted:

Deleted:

Deleted: Fig.

Plant functional types

In this model, we use a set of continuous plant traits to define plant functional types, so that we can simulate plant emergent properties (such as dominant plant types, vegetation compositional changes, etc.) in response to climate changes based on the underlying plant physiological properties and ecological principles through eco-evolutionary modeling in the future. For example, life forms are defined by the continuums characterized by wood density (woody vs. herbaceous), height growth coefficient (tree vs. shrub), and leaf mass per unit area (LMA, for evergreen vs. deciduous). Deciduousness is defined by cold resistance (evergreen vs. cold deciduous), and drought resistance (evergreen vs. drought deciduous). Grasses are simulated as

tree seedlings with all stems senescent along with leaves at the end of a growing season. The individuals are reset back to their initial sizes each year and the population density is also reset by conserving current total biomass. The photosynthesis pathway is predefined as C_3 or C_4.

Table 1 Plant functional types used in BiomeE

Plant functional types	V_{cmax}	LMA (kg C m^{-2})	$L_{max,0}$	ρ_W (kg C m^{-3})	α_Z	$T_{0,c}$	$\beta_{0,D}$	PS pathway
1. Tropical evergreen broadleaf	18	0.07	4.8	360	30	15	0	C_3
2. Temperate/boreal evergreen needleleaf	18	0.14	4.8	300	30	-80	0	C_3
3. Temperate/boreal deciduous broadleaf	22	0.025	4.5	350	30	15	0	C_3
4. Tropical drought deciduous broadleaf	20	0.03	4.5	250	30	15	0.2	C_3
5. Boreal deciduous needleleaf	20	0.03	4.0	300	30	15	0.0	C_3
6. Cold shrub	18	0.025	3.0	360	20	15	0.1	C_3
7. Arid shrub	18	0.03	3.0	360	20	15	0.1	C_3
8. C3 grass	20	0.025	2.5	90*	10	5	0.2	C_3
9. C4 grass	15	0.025	2.5	90*	10	5	0.2	C_4

V_{cmax}: leaf maximum carboxylation rate, LMA: leaf mass per unit area, $L_{max,0}$: is crown maximum leaf area index, ρ_W: wood density, α_Z: Height coefficient, $T_{0,c}$: Critical temperature for phenology offset, $\beta_{0,D}$: critical soil moisture index for the offset of phenology, PS: photosynthesis pathway, E: evergreen, C: cold-deciduous, D: drought-deciduous. *Grass stem density is calculated as tissue biomass divided by stem volume. The tissue density of grass's stems is as high as wood.

We defined 9 PFTs for our test runs in this paper to roughly represent global vegetation functional diversity (Table 1) according to their life form (tree, shrub, and grass), photosynthesis (C_3 and C_4), and leaf phenology (evergreen and deciduous). Crop PFTs were not included because the purpose of this paper is to describe the baseline processes of natural vegetation and soil biogeochemical cycle. These PFTs have the same physiological and demographical processes with different parameters (except C_3 and C_4 photosynthesis pathways) representing

Deleted: using the

Deleted: of current cohort and predefined initial size of grasses…

Formatted: Right: 0"

varied strategies in different environments. Thus, for eco-evolutionary and ecological community assembly simulations, one PFT can switch to another by changing its parameters for searching competitively optimal plant traits in different environments.

Phenology

The phenology types are defined by two parameters, a critical low temperature and a critical soil moisture index, that are used to trigger leaf fall. These two parameters define 4 phenological types with their possible factorial combinations: evergreen, drought-deciduous, cold-deciduous, and drought-cold-deciduous. Evergreen PFTs have high resistances to cold (i.e., very low critical temperature) and drought (very low soil drought). Cold and drought deciduous PFTs have low critical temperature and soil drought index, respectively. These phenological types represent different strategies of dealing with environmental stresses and pressure of competition. It is possible that the evergreen would be more competitive in high seasonality regions (e.g., evergreen in boreal regions), though the first response of plants to harsh environments (e.g., cold or dry) is to shed their leaves. Our definition of phenology is designed to allow to evaluate the competitively optimal strategy in future studies.

For the cold-deciduous PFTs (temperate/boreal deciduous broadleaf and cold shrub), we used the growing degree days above 5 °C (GDD_5) to trigger phenological onset and a critical low temperature (T_m) for the offset. GDD_5 is calculated from the days that temperature starts to increase from the coldest days in the non-growing season. The critical value of GDD that the plants require for growth (GDD_c) is defined as a function of chilling days in the non-growing season (Prentice et al., 1992):

$$GDD_c = a_0 + d \cdot e^{-b \cdot N_{CD}}, \quad (1)$$

Deleted: P

Deleted: make it possible

Deleted: 3

Deleted: 5

Deleted: control the timing of

Deleted: to control

Formatted: Font: Italic

where, N_{CD} is the days of the cold period in nongrowing season before bud burst, a_0 is the minimum GDD_c (50) when the cold period is sufficiently long, d is the maximum addition of GDD_c (800) when there is no cold period (i.e., N_{CD}=0), b is a shape coefficient (0.025). These parameters are tunable and should change with acclimation to new climates.

The running mean temperature that represents the mean temperatures over a short period of time is calculated as:

$$\begin{cases} T_m(i) = T_d(i), & when\ i = 1 \\ T_m(i) = 0.8T_m(i-1) + 0.2T_d(i), & when\ i \geq 2 \end{cases}, \quad (2)$$

The critical temperature of triggering leaf senescence (T_c) is calculated as a function of the number of growing days (N_{GD}).

$$T_c = T_{0,c} - s \cdot e^{-c\cdot(\max(0, N_{GD} - L0))}, \quad (3)$$

where, $T_{0,c}$ is the highest critical temperature when N_{GD} is sufficiently long, s is the range that a critical temperature can change, c is a shape parameter, $L0$ defines the lowest critical temperature ($T_{0,c}$ -s) when N_{GD} is smaller than $L0$. The rationale in this equation is that when a growing period is not long enough, plants need a lower T_c to trigger leaf fall so that they can have a growing season that is not too short. This setting is based on the thermal adaptation analysis of Yuan *et al.* (2011).

For the drought deciduous PFTs (tropical drought deciduous broadleaf, arid shrub, C_4 grass), we used a soil moisture index (s_D) to start and end a growing season.

$$s_D = \sum_{i=1}^{n} Min\left(1.0, max\left(\frac{\theta_i - \theta_{WP,i}}{\theta_{HC,i} - \theta_{WP,i}}, 0.0\right)\right), \quad (4)$$

Formatted: Indent: First line: 0.38"

Deleted: We used an index of cold condition (accumulative low temperature, ALT) to make sure the low temperature signal is persistent and differentiates the signal of the seasonal temperature changes and the stochastic low temperature stresses in growing seasons.

Deleted: for

where i is the soil layer in root zone, θ is soil water content (vol./vol.), θ_{WP} is wilting point, and θ_{HC} is soil water holding capacity. The critical soil moisture values that trigger new leaf growth and leaf fall are defined as PFT-specific parameters. We slightly tuned these two parameters according to the soil moistures where the deciduous PFTs' leaves start to grow or fall. Usually, the critical soil moisture for starting new leaf growth is higher than the soil moisture levels that trigger leaf senescence so that the plants can have a stable growing season.

Deleted: fall

Plant demography and biogeochemical cycles

Allometry and Plant architecture

The plant allometry and architecture are critical for plant resources allocation, light capture, and soil water and nutrients uptake. The allometry equations are the same as those used in LM3-PPA (Farrior et al., 2013; Weng et al., 2015):

$$\begin{cases} A_C = \alpha_C D^{\theta_C} \\ Z = \alpha_Z D^{\theta_Z} \\ S = 0.25\pi\rho\Lambda\alpha_H D^{2+\theta_H} \\ A_L^* = l_{max} A_C \\ A_{FR}^* = \varphi_{RL} l_{max} A_C \end{cases}, \quad (5)$$

where D is tree diameter; A_C is crown area; Z is plant height; S is woody biomass (sapwood plus heartwood); α_C and α_Z, are the scaling factors for crown area and plant height, respectively; θ_C and θ_Z are the exponents for crown area and tree height, respectively; π is ratio of a circle's circumference to its diameter; ρ is wood density (kg C m^{-3}); Λ is the taper factor from a cylinder to a tree with the same D; A_L^* and A_{FR}^* are the target surface area of leaves and fine roots, respectively; φ_{RL} is the area ratio of leaves to roots. l_{max} is the maximum leaf area per unit crown area, defined as a function of plant height (Z):

$$l_{max}(Z) = L_{max,0}(Z + h_0)/(Z + H_0), \quad (6)$$

where $L_{max,0}$ is the maximum crown LAI when a tree is sufficiently tall, Z is tree height, h_0 is a small number that makes a minimum l_{max} ($L_{max,0}$ (h_0/H_0)) when tree height is close to zero, and H_0 is a curvature parameter.

Plant growth and allocation of carbon and nitrogen to plant tissues

The allocation of carbon to wood, leaves, and roots is affected by climate and forest age (Litton et al., 2007; Xia et al., 2019). However, vegetation models cannot capture these patterns well at large spatial scales, even if the adaptive responses to climate and forest ages are considered (Xia et al., 2019, 2017), partly because of the absence of explicit representation of shifts in species composition and competition between individuals (Franklin et al., 2012; Dybzinski et al., 2015). BiomeE has an optimal growth scheme that drives the allocation of carbon and nitrogen to leaves, fine roots, and stems based on the optimal use of resources and light competition (Weng et al., 2019). In this scheme, the growth of new leaves and fine roots follows the growth of woody biomass (i.e., stems), and the area ratio of fine roots to leaves is kept constant during the growing season. The allocation of available carbon between structural (e.g., stems) and functional (e.g., leaves and fine roots) tissues is optimal for light competition at given nitrogen availability.

Deleted: NPP

Mathematically, differentiating the stem biomass allometry in Eq. 5 with respect to time, using the fact that dS/dt equals the carbon allocated for wood growth (G_W), gives the diameter growth equation:

$$\frac{dD}{dt} = \frac{G_W}{0.25\pi\Lambda\rho_W\alpha_z(2+\theta_z)D^{1+\theta_Z}} \quad (7)$$

This equation transforms the carbon gain from photosynthesis to the diameter growth that results from wood allocation and allometry (Eq 5). With an updated tree diameter, we can calculate the new tree height and crown area using allometry equations, and the targets of leaf and fine root biomass (Eq. 5). Generally, the growing-season average allocations of carbon and nitrogen to different tissues are governed by two parameters: the maximum leaf area per unit crown area (l_{max}) and fine root area per unit leaf area (φ_{RL}) (Eq. 5). The optimal-growth allocation scheme combined with explicit competition for light and soil resources in our model makes it possible to simulate the underlying processes that determine emergent allocation patterns (Dybzinski et al., 2011; Farrior et al., 2013; Farrior, 2019; Weng et al., 2019).

Reproduction and Mortality

At a yearly time-step, the cumulative carbon and nitrogen allocated for reproduction by a canopy cohort over the growing season length, *T,* is converted to seedlings according to the initial plant biomass (S_0) and germination and establishment probabilities (p_g and p_e, respectively). Generally, the population dynamics can be described by a variant of the von Foerster equation (von Foerster, 1959):

$$N(S_0,t) = \frac{p_g p_e}{s_0}\int_0^T N(\tau)G_F(\tau)d\tau$$
$$\frac{dN(s,t)}{dt} = -\mu(s,t)N(s,t). \quad (8)$$

where $N(S_0, t)$ is the spatial density of newly generated seedlings, $N(\tau)$ is the spatial density of this cohort of trees at time τ, G_F is the carbon allocation to seeds, and μ is PFT-specific mortality parameter.

Each PFT has a canopy-layer-specific background mortality rate that is assigned from the literature. These background rates are assumed to be size-independent for the canopy layer trees,

but size-dependent for understory trees. Many factors affect tree mortality, such as light, size, competition crown damage, hydraulic failure, trunk damage etc. (Lu et al., 2021; Zuleta et al., 2022). These factors result in high mortality rates of seedlings and old trees (i.e., a "U-shaped" mortality curve). We use the following equation to delineate a mortality rate that varies with social status (crown layers), shade effects, and tree sizes:

$$\mu(s,t) = \mu_0(1 + f_L f_s) f_D \quad (9)$$

where f_L is the shade effects on mortality ($f_L = \sqrt{L-1}$), f_S is seedling mortality when a tree is small ($f_s = A_{SD} e^{-B_{SD} \cdot D}$), and f_D represents the size effects on the mortality of adult trees ($f_D = m_s \frac{e^{A_D(D-D_0)}}{1+e^{A_D(D-D_0)}}$). L is the layer this plant is in (L=1 for the canopy layer and 2 for the second, and so on), A_{SD} is the maximum multiplier of mortality rate for the seedlings in the understory layers, B_{SD} is the rate of mortality decreasing as tree diameter (D) increases, m_s is the maximum multiplier of mortality rate for large-sized trees, D_0 is the diameter at which the mortality rate increases by m_s /2, and A_D is a shape parameter (i.e., the sensitivity to tree diameter).

Crown self-organization and layering

Tree crowns are arranged into different vertical canopy layers according to tree height and crown area if their total crown area is greater than the land area following the rules of the PPA model (Strigul et al., 2008). In PPA, individual tree height is defined as the height at the top of the crown, and all leaves of a given cohort are assumed to belong to a single canopy layer. The height of canopy closure for the top layer is referred to as critical height (Z^*, the height of the shortest tree in the layer) and is defined implicitly by the following equation:

$$k(1-\eta) = \sum_i \int_{Z^*}^{\infty} N_i(Z,t) A_{CR,i}(Z^*, Z) dZ \quad (10)$$

where $N_i(Z,t)$ is the density of PFT i trees of height Z per unit ground area; $A_{CR,i}(Z^*,Z)$ is the crown area of an individual PFT i tree of height Z; η is the proportion of each canopy layer that remains open on average due to wind and imperfect spacing between individual tree crowns, and k is the ground area. The top layer includes the tallest cohorts of trees whose collective crown area sums to $1-\eta$ times the ground area; lower layers are similarly defined.

All the trees taller than the critical height can get full sunlight and all trees below this height are shaded by the upper layer trees. Trees within the same layer do not shade each other, but there is self-shading among the leaves within individual crowns. Cohorts in a sub-canopy layer are shaded by the leaves of all taller canopy layers. In each canopy layer, all cohorts are assumed to have the same incident radiation on the top of their crowns. Note, the gap fraction η is necessary to allow additional light penetration through each canopy layer for the persistence of understory trees in monoculture forests in which the upper layer crowns build a physiologically-optimal number of leaf layers (Farrior et al., 2013). The grasses only form one layer. Those individuals who cannot stay in that layer because of limited space will be killed (i.e., when the total grass crown area is larger than the land area).

Ecosystem carbon and nitrogen biogeochemical cycles

Ecosystem biogeochemical cycles (carbon and nitrogen in this model) are driven by plant and microbial demographic processes. There are seven pools in each plant: leaves, fine roots, sapwood, heartwood, fecundity (seeds), and non-structural carbohydrates and nitrogen (NSC and NSN, respectively). The carbon and nitrogen in plant pools enter soil pools with the mortality of individual trees and the turnover of leaves and fine roots. Soil has a mineral nitrogen pool for mineralized nitrogen and five soil organic matter (SOM) pools for carbon and nitrogen:

metabolic litter (x_1), structural litter (x_2), microbial (x_3), and fast (x_4) and slow-turnover (x_5) SOM pools.

The microbial pool plays a central role in the transfer and decomposition of SOM. The decomposition processes are simulated by a model modified from Manzoni et al. (2010). The technical details have been described in Weng et al. (2019, 2017). The decomposition rate of a SOM pool is determined by the basal turnover rate together with soil temperature and moisture following the formulation of the CENTURY model (Parton et al., 1988, 1987). The microbial carbon use efficiency (transfer from litter to microbial matter) is a function of litter nitrogen content, following the model of Mazoni et al. (2010).

The N mineralization in decomposition is determined by microbial nitrogen demand, SOM's C:N ratio, and decomposition rate. In the high C:N ratio SOM, microbes must consume excess carbon to get enough nitrogen for growth. By contrast, in the low C:N ratio SOM, microbes must release excess nitrogen to get enough carbon for energy. Depending on the C:N ratios of SOM, soil microbes may be limited by either C or N.

The out-fluxes of C and N from the i^{th} pool (dC_i and dN_i, respectively) are calculated by:

$$\begin{aligned} dC_i &= \xi(T,M)\rho_i QC_i, \\ dN_i &= \xi(T,M)\rho_i QN_i , \end{aligned} \tag{11}$$

where ξ is the response function of decomposition to soil temperature (T) and moisture (M), ρ_i is the basal turnover rate of the i^{th} litter pool at reference temperature and moisture, QC_i is the C content in i^{th} pool, and QN_i is the N content in the i^{th} pool.

The new microbial growth (dM) is calculated as the co-limit of available carbon and nitrogen mobilized at this step:

$$dM_i = Min(\varepsilon_0 \cdot dC_i, \Lambda_{microbe} \cdot dN_i), \quad (12)$$

where ε_0 is default carbon-use efficiency of litter decomposition (0.4) and Λ_{microbe} is a microbe's C:N ratio, which is a fixed value (10 in this model). The soil heterotrophic respiration (R_h) is the microbial respiration (i.e., the difference between carbon consumption and new microbial growth), and the total N mineralization rate ($N_{\text{mineralized}}$) is calculated as the sum of mineralized N in the SOM pools and microbial turnover:

$$R_h = \sum_{i=3}^{5} dC_i - \sum_{i=4}^{5} M_i,$$
$$N_{mineralized} = \sum_{i=3}^{5} dN_i - \sum_{i=3}^{5} m_i/\Lambda_{\text{microbe}} \quad (13)$$

The R_h releases to atmosphere as CO_2. Mineralized N enters the mineral N pool for plants to use. The dynamics of the mineral N pool is represented by the following equation:

$$\frac{dN_{mineral}}{dt} = N_{deposition} + N_{mineralized} - U - N_{loss}, \quad (14)$$

where $N_{\text{deposition}}$ is N deposition rate, assumed to be constant over the period of simulation; N_m is the N mineralization rate of the litter pools (fast and slow SOM and microbes); U is the N uptake rate (Kg N m^{-2} $hour^{-1}$) of plant roots; and N_{loss} includes the loss of mineralized N by denitrification and runoff. The N deposition ($N_{\text{deposition}}$) is the only N input to ecosystems, and we set nitrogen fixation as zero in this version of the model.

3 Model Test runs

For our comparison of model performance against observations and other models, we used the full demographic version of BiomeE (described above) and also designed a "single-cohort" version of the model to benchmark our demographic implementations. In the single-cohort model, the mortality of trees is simulated as the turnover of woody biomass, and the fecundity

Formatted: Indent: First line: 0.38", Line spacing: Double

resources (carbon and nitrogen) are used to build the same-sized parent trees, instead of seedlings growing from understory layers. If the total crown area of the trees in this cohort is greater than the land area, the extra trees will be removed to make the total crown area less than or equal to the land area. At equilibrium, the turnover of woody biomass is equal to the new growth each year and the new trees generated from fecundity resources are killed by self-thinning. The single-cohort model uses the mean state of the canopy layer trees to represent the characteristics of the whole community. This single-cohort model performs like the traditional biogeochemical models and simplifies vegetation computation.

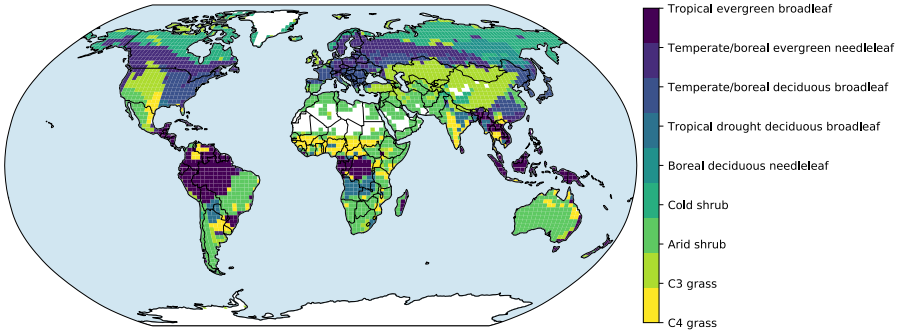

Figure 2. Prescribed global distribution of plant functional types. Data is from the Ent Global Vegetation Structure map.

In the test runs, the distribution of PFTs was obtained from the Ent vegetation map (Ito et al., 2020), which was derived from 2004 MODIS land cover and PFT data products (Friedl et al., 2010) and climate data (Figure 2). For these simulations, croplands and pastures were replaced by the potential natural vegetation types. We slightly tuned leaf maximum carboxylation rate (V_{cmax}) to fit the general pattern of global GPP, while keeping other parameters unchanged.

Deleted: ¶

Deleted:

Deleted: is

Deleted: Fig.

Forcing data are from the TRENDY project CRU-NCEP data (Sitch et al., 2015) and have a 6-hour time step at a spatial resolution of 0.5°x0.5°. These data are available at the website https://www.uea.ac.uk/web/groups-and-centres/climatic-research-unit/data.

We aggregated these data into 2.0°x2.5° grid cells and used thirty years' of data (1988~2017) to force the model to run for 600 years, which is long enough for the model to approach equilibrium states for both vegetation and soil carbon pools. These data include temperature, precipitation, shortwave radiation, longwave radiation, specific humidity, and wind speed (U and V directions). We interpolated the radiation data (R_S) into half-hour timesteps based on the sun zenith angle (θ_S) and radiation penetration rate calculated from data.

$$R_S(t) = \left(\frac{R_{H6}}{S^* cos cos\, \theta_S(H6)}\right) S^*\, cos\, cos\, \theta_s(t) \ , \qquad (15)$$

where S^* is solar constant (1362 W/m^2). Other variables are linearly interpolated to the model time steps, which is half hourly in this study. Atmospheric CO_2 concentration is set at the model default level (350 ppm) in our model runs.

Data sources for model evaluation

The LAI data were from the Ent vegetation dataset (Ito et al., 2020), where the LAI was derived from 2004 MODIS LAI data (Tian et al., 2003, 2002). **Gross primary productivity (GPP) data** are from a global retrieval of GPP using remote sensing observations. These data are on a 1°×1° geographic grid at a monthly time step based on an Artificial Neural Network retrieval algorithm (Alemohammad et al., 2017). This algorithm uses six remotely sensed observations as input: Solar Induced Fluorescence (SIF), Air Temperature, Precipitation, Net Radiation, Soil Moisture, and Snow Water Equivalent. The data are available from 2007 to 2015. **The tree height data** are from spaceborne light detection and ranging (lidar) global map of canopy height at 1-km spatial

Deleted: ¶

Formatted: Font: Bold

Deleted: surface turbulent fluxes including latent heat, sensible heat, and

480 resolution developed by Simard et al. (2011). These authors used the 2005 data from the
481 Geoscience Laser Altimeter System (GLAS) aboard ICESat (Ice, Cloud, and land Elevation
482 Satellite) to derive global forest canopy heights. **Biomass data** are from a Global 1-degree Maps
483 of Forest Area, Carbon Stocks, and Biomass, 1950-2010 developed by Hengeveld et al. (2015).
484 **Soil carbon data** are from Food and Agriculture Organization (FAO) Harmonized World Soil
485 Database (version 1.2), updated by Wieder et al. (2014).

486 **MsTMIP model simulation data**

487 We chose six model simulations (BiomeBGC, CTEM, CLM4, LPJ, Orchidee, VEGAS) from the
488 Multi-scale Synthesis and Terrestrial Model Intercomparison Project (MsTMIP) (Huntzinger et
489 al., 2013) to compare against our model simulations. These models are well-developed and
490 widely used in Earth system models, representing the state-of-art of current land vegetation
491 model development. MsTMIP provided prescribed land use types for all the participant models.
492 However, it is up to the participant models to simulate disturbance impacts on ecosystems
493 (Huntzinger et al., 2013). MsTMIP conducted five sets of experimental runs with different
494 climate forcing, land-use history, atmospheric CO_2 concentration, and nitrogen deposition. In
495 this study, we compared to the SG1 simulation experiment because it is driven by the 1901~2010
496 climate forcing data with constant CO_2 concentration and constant land cover (Huntzinger et al.,
497 2013), which are the closest to our model runs.

498 **Selected Grid Cells for Comparison**

499 To illustrate model behavior, we selected 8 grid cells that cover boreal forests, temperate
500 forests, tropical forests, C_4 grasslands, and arid shrublands to show the simulated ecosystem
501 development patterns across the climate zones with different dominant PFTs (Table 2). Brazil
502 Tapajos (TPJ), Oak Ridge (OKR), Harvard Forest (HF), Manitoba old black spruce site (MNT),

Deleted: for

Deleted: used

and Bonanza Creek (BNC) are covered by tree PFTs. Konza long-term ecological research station (LTER) (KZ) is C_4 grass. Walnut Gulch Kendall (WGK) and Sevilleta LTER (SV) are covered by arid shrubs. These sites were chosen because they have extensive data on vegetation and climate conditions for future comparisons.

Table 2 Sites for simulated ecosystem development illustration

Site	Dominant PFT	Coordination	Mean Temperature (°C)	Annual Precipitation (mm)
Bonanza Creek (BNC)	Broadleaf deciduous	63.92°, -145.38°	-3.1	269
Manitoba old black spruce site (MNT)	Evergreen needleleaf	55.88°, -98.48°	-3.2	520
Harvard Forest (HF)	Broadleaf deciduous	42.54°, -72.17°	8.5	1050
Oak Ridge (OKR)	Broadleaf deciduous	35.96°, -84.29°	13.7	1372
Konza LTER (KZ)	C_4 grass	39.08°, -96.56°	12.4	835
Sevilleta LTER (SV)	Arid shrub	34.36°, -106.88°	12.7	365
Walnut Gulch Kendall (WGK)	Arid shrub	31.74°, -109.94°	17.7	350
Brazil Tapajos (TPJ)	Broadleaf evergreen	-2.86°, -54.96°	26	1820

4 Results

4.1 Simulated vegetation structural and ecosystem carbon dynamics

In the forest sites, the simulated vegetation structure by the full demographic model changes with the growth, regeneration, and mortality processes (Figure 3). The temporal dynamics of the canopy development can be separated into three stages according to the canopy crown dynamics: 1) open forest stage, 2) self-thinning stage, and 3) stabilizing stage. In the open forest stage, the crown area index (CAI) is less than 1.0 and all the individuals are in full sunlight. The tree crowns grow rapidly to occupy the open space (Figure 3: a). In the self-thinning stage, the open

Deleted: K

Deleted: Fig.

Deleted: It

Deleted: Fig.

space is filled by the crowns of similar sized trees (i.e., the forest is closed) and canopy trees are continuously pushed to the lower layer(s) (i.e., self-thinning) and the CAI continues to increase due to the limited space with growing tree crowns (i.e., the new spaces vacated from the canopy trees' mortality cannot meet the space demand from crown growth). The sizes of trees in the canopy layer are still similar in this period (Figure 3: b and c) and the critical height (the height of the shortest tree in the canopy layer) keeps increasing in this period. In the stabilizing stage, when the space generated by the mortality of canopy trees is larger than the growth of canopy tree crown area, no trees are pushed to the lower layer and the lower layer trees start to enter the canopy layer and fill the space, leading to a sharp decrease in critical height (Figure 3: b) and the mixing of different sized trees in the canopy layer. The CAI is decreasing as well because of the high mortality rates of the understory layer trees. As time goes on, the growth, regeneration, mortality, and space filling processes are equilibrated, and the forest structure is then stabilized.

The tallest plant height (Figure 3: c) shows the height of the trees in the tallest cohort. It keeps growing as this cohort exists. The sharp decreases indicate the replacements by or merging with another shorter cohort because the density of trees in this cohort is very low (0.0001/ha in this case) or the similarity between the tallest and the second tallest is high. The total basal area (Figure 3: d) is an index of the sum of all trees at a site. It keeps increasing during forest development and is equilibrated earlier than height and crown structure.

Deleted: Fig.

Deleted: Fig.

Deleted: Fig.

Deleted: Fig.

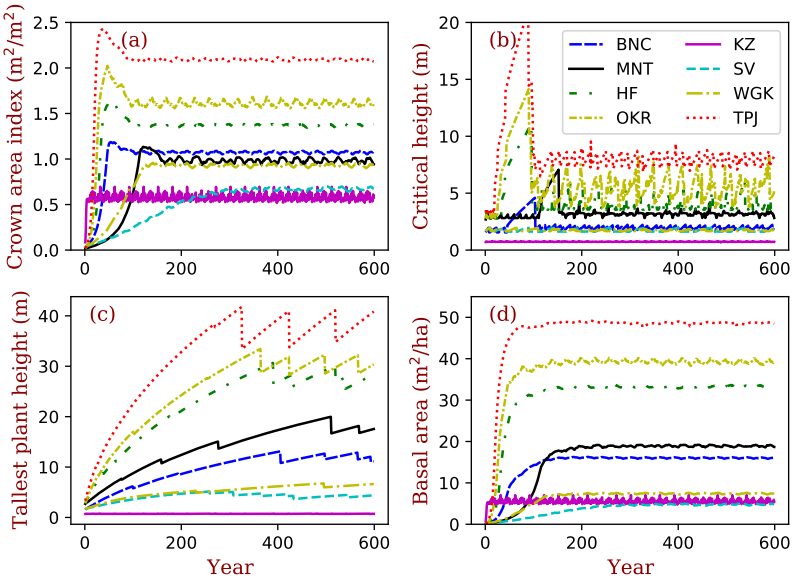

Figure 3. Vegetation structural dynamics with the full demographic BiomeE at the field sites listed in Table 2. Critical height is an index of the model PPA, which separates the trees that are in full sunlight if taller than critical height and those that are fully shaded if shorter than critical height.

Among these sites, at equilibrium, the tropical forest site (TPJ) has the highest crown area index (around 2.2), followed by warm temperate forest at OKR, mixed forest at HF, and boreal forests at BNC and MNT (Figure 3). The shrubs and grasslands in arid regions have the lowest crown area index (CAI), with basal area following similar patterns. For forested sites, tree height is tallest at TPJ, followed by OKR, HF, MNT, and BNC. The shrubs are short according to their allometry parameters and the height of grasses during non-growing season is zero. The critical height, which separates canopy layer trees from the understory layers, follows the same order as

Deleted: Fig.

that of tree height with high fluctuations with cohort changes. (More cohort details are in Supplementary Information Figures S1-S8)

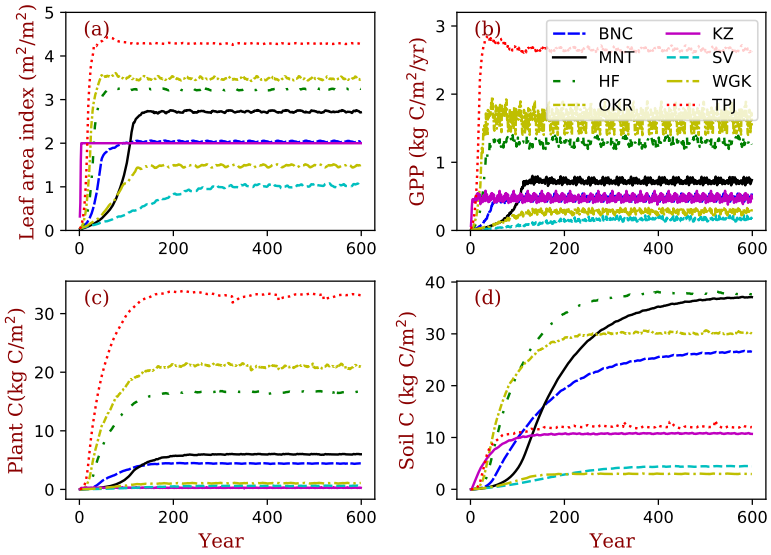

Figure 4: Site ecosystem development simulated by BiomeE with full demography for the field sites listed in Table 2

For the temporal dynamics in the full demographic simulations (Figure 4), the simulated GPP aligns closely with LAI and they reach their equilibrium states at similar times across sites (Figure 4: a,b). According to the definition of maximum crown LAI (l_{max}) in Eq. 6, the grass LAI (i.e., Konza) reaches the maximum each year, except the first year due to the low initial density (Figure 4: a). The biomass accumulation is much slower in forests because of the longer time needed for forest structure (size distribution) to reach equilibrium. Soil carbon equilibration is faster in the warm regions than in cold regions overall because of the higher turnover rate of SOM pools in warm regions. At equilibrium, forested sites have higher LAI,

Deleted:

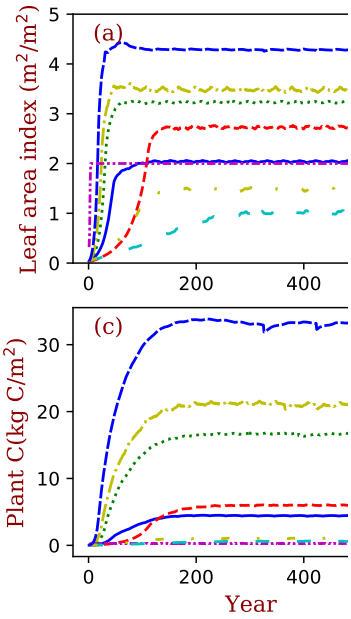

Deleted: Fig.

Deleted: Fig.

Deleted: Fig.

biomass, and carbon stocks per area compared to the shrub and grass sites overall. Vegetation biomass is lowest at the grassland site, Konza LTER, because, within the model, grassland ecosystems cannot accumulate persistent woody biomass.

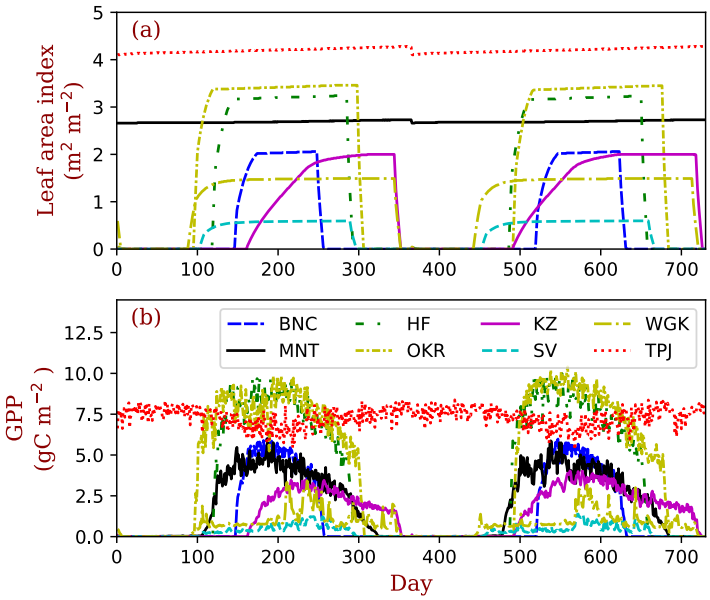

Figure 5. Seasonal patterns of LAI and gross primary production in the sample grids. Two years of data are shown in this figure. The key to location abbreviations is in Table 2.

The PFTs at TPJ and MNT are evergreen trees. Their LAI does not change over the whole year (Figure 5: a). The forest in OKR has the longest growing season in the three deciduous forest grids, followed by HF and BNC. BNC's growing season is only around 120 days, about half of OKR's growing season. The growing season of grasses in KZ starts in late May and ends in September. The two arid-adapted shrub sites (SV and WGK) are controlled by water availability. In TPJ (tropical evergreen forest), the trees have photosynthesis throughout the

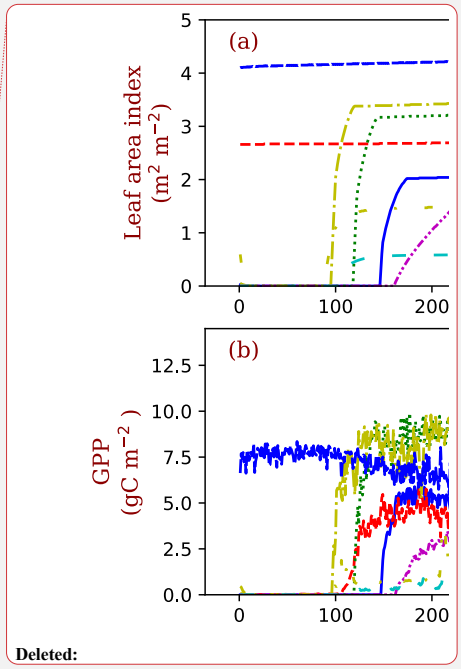

Deleted:

Deleted: Fig.

Deleted: WKG

entire year (Figure 5: b). In MNT, photosynthesis only happens in warm seasons with the leaves kept in the crowns (evergreen needleleaf). The deciduous trees in OKR and HF have high photosynthesis rates during the growing season. The photosynthesis rates in SV and WGK are generally low because of the dry environments. However, the precipitation events can drive photosynthesis rates high in these arid regions.

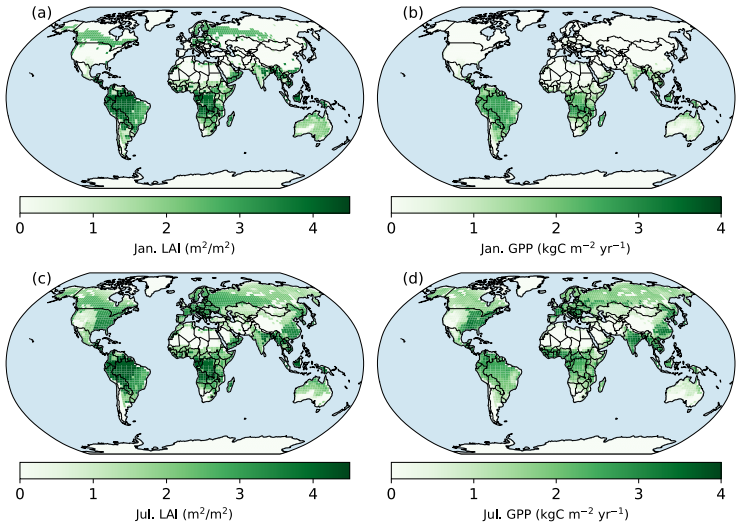

Figure 6. Spatial patterns of LAI and GPP in Jan and July simulated with full demography setting. Panels a and b are the LAI and photosynthesis of January in the year of 600 (the last year of model run). Panels c and d are July's in the same year.

At the global spatial scale, only evergreen needle-leaved forests keep their leaves in northern high latitude regions during January (Figure 6), though photosynthesis in this region ceases because of the low temperature. In July, northern high latitude regions green up and their photosynthesis rates are high in wet regions. The single cohort BiomeE predicted similar pattern because the phenology model is same (Figure S9).

Deleted: Fig.

Deleted: WKG

Deleted: Fig.

4.2 Global Comparisons with Observations

The simulated LAI roughly capture the spatial pattern of MODIS LAI (Figure 7: a and b), though there are high variations at each grid (Figure 8: a). Generally, the simulated LAI in well vegetated grids, e.g., boreal forest regions, is underestimated by our model because the crown LAI is calculated as a function of tree height and a parameter of maximum crown LAI (Table 1 and Eq. 6). The LAI in the grids that were converted to different land use types is overestimated because we assume all terrestrial grids are covered by potential vegetation in our test runs. Compared with SIF GPP (Alemohammad et al., 2017), simulated GPP is higher than the SIF GPP generally, though lower in arid regions (Figure 7: c, d and Figure 8: b). The simulated tree height (Figure 7: e, f and Figure 8: c) is mostly taller compared to observations (Simard et al., 2011) because most forests have been altered by human activities (Pan et al., 2013). However, the model and observations cover approximately the same range of tree heights (up to 40 m). Simulated biomass is much higher than the observations (Figure 7: g, h and Figure 8: d) because, in the observations, many forest regions have been transformed to low biomass land use types (such as croplands) or represent earlier successional stages with less accumulated carbon (i.e., not equilibrium states).

Simulated soil carbon does track the observations (Figure 7: i, j and Figure 8: e) better than biomass, likely because soil carbon stocks are more stable compared to biomass in response to disturbances and human activities. For areas where the model underpredicts soil carbon, the difference could arise from the missing biogeochemical processes that may lead to high carbon accumulation in some regions (e.g., peats) (Davidson and Janssens, 2006; Briones et al., 2014;

Deleted: We tuned the parameter of maximum carboxylation rate (V_{cmax}) to fit the general pattern of global GPP.

Deleted: (Figs. 7 and 8)

Deleted: (Fig. 7)

Deleted: g

Deleted: and

Deleted: h

Deleted: ; and GPP does not change much compared to the changes in vegetation biomass because leaves can reach to equilibrium much faster than the biomass does (Fu et al., 2017)…

644 Euskirchen et al., 2014) and the relatively high uncertainties in the soil carbon data (Tifafi et al.,
645 2018).

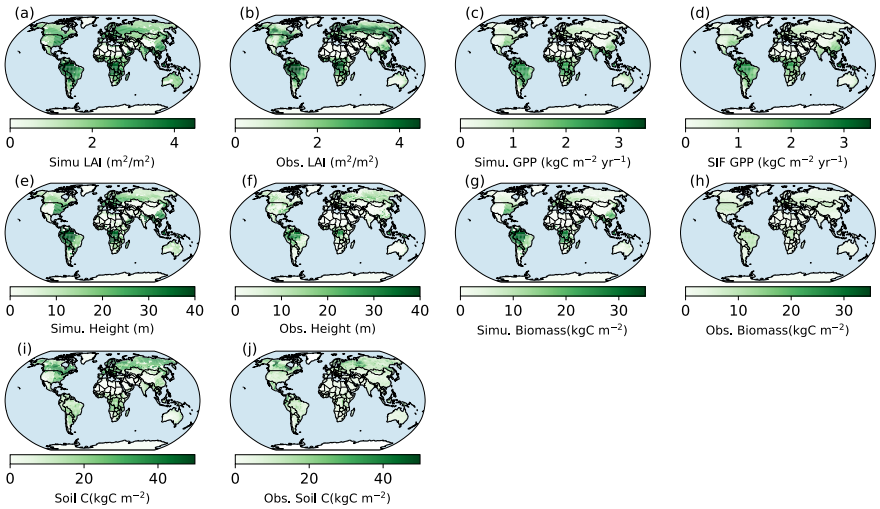

646

647 **Figure 7. Spatial patterns of BiomeE (full demography) simulations and those from data**.
648 "Obs." means different ways retrieved from observations. Obs. LAI is from Ent vegetation data
649 (Modis LAI 2004) (Ito et al., 2020; Tian et al., 2003). Obs. **GPP is** derived from Solar Induced
650 Fluorescence (SIF) data with a machine learning approach (Alemohammad et al., 2017). The
651 data are available from Jan. 2007 to Dec. 2015. **The tree height data** are from spaceborne light
652 detection and ranging (lidar) global map of canopy height at 1-km spatial resolution developed
653 by Simard et al. (2011). **Biomass data** are from Hengeveld et al. (2015). **Soil carbon data** are
654 from FAO Harmonized World Soil Database (version 1.2), updated by Wieder (2014).

655

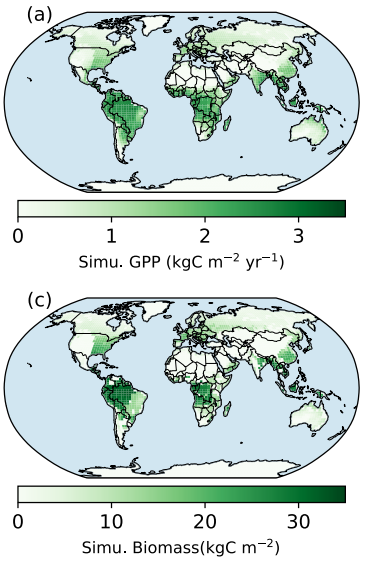

Deleted:

Formatted: Left

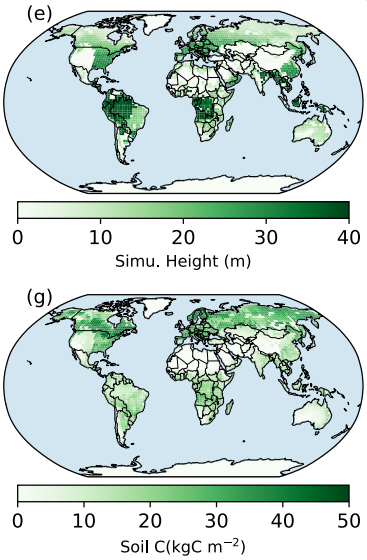

Deleted:
Figure 7. Spatial patterns of BiomeE (full demography) simulations and those from data. "Obs." means different ways retrieved from observations. Obs. Some are mod ... [1]

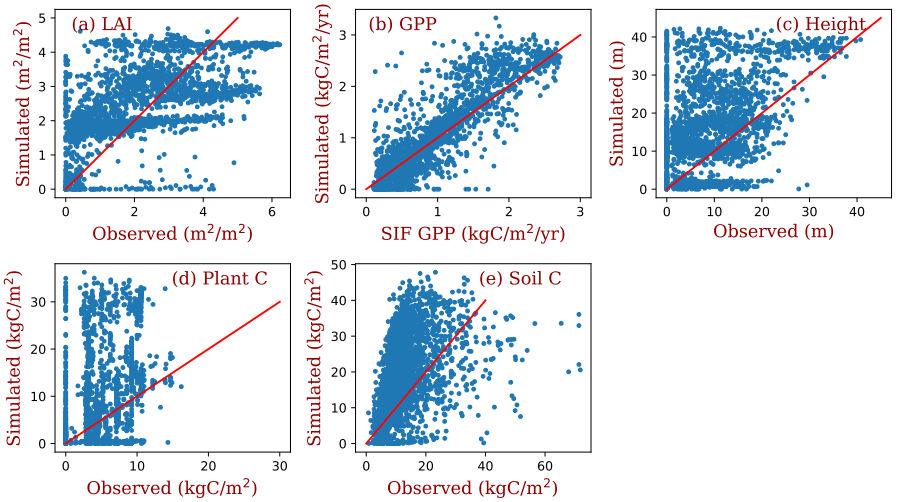

676

677 **Figure 8**. **Grid comparison of full demographic BiomeE simulations with observations**
678 **estimates**. The red line in each panel is the 1:1 line. This figure uses the same data as those in
679 Figure 7.

680

681 **4.3 Comparison with MsTMIP models**

682 We compared the performance of our model with MsTMIP models at the 8 locations that were
683 used to show ecosystem development patterns (Table 2). For most of these sites, LAI in BiomeE
684 is lower compared the other MsTMIP models (Figure 9: a), while the estimated GPP is within
685 the range of MsTMIP predictions (Figure 9: b). LAI differences are a consequence of the
686 formulations within BiomeE, as described further in the Discussion (5.2 Model predictions and
687 performance). Specifically, BiomeE simulates leaf growth by using a maximum crown LAI,
688 which is lower than the real forest LAI.

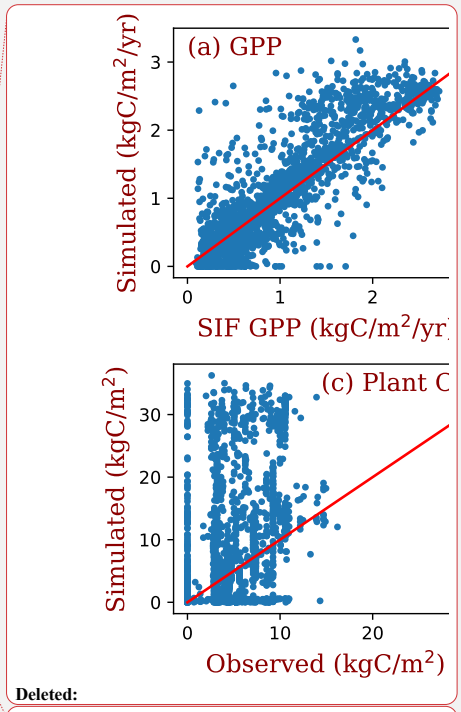

Deleted:

Deleted: simulated and observed

Deleted: of

Deleted: Fig.

Deleted: Fig.

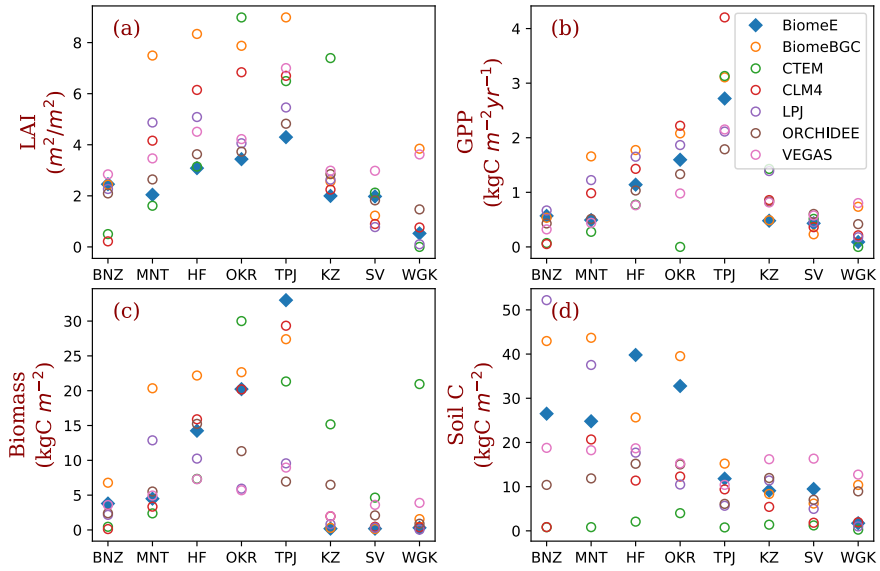

694

695 **Figure 9 Site-level comparison with MsTMIP models**.

696 The BiomeE predictions are from the full demography. The abbreviations of the 8 sites
697 (corresponding to model grid cells) and their coordination, dominant PFTs, and climatic
698 conditions are in Table 2. (See Figures S12 and S13 in Supplementary Information for the single
699 cohort BiomeE simulations.)

700

701 The low LAI does not affect crown total photosynthesis because leaves in lower canopy
702 layers contribute little to the total carbon assimilation. BiomeE predicted biomass (Figure 9: c)
703 and soil carbon (Figure 9: d) generally fall towards the higher end of the MsTMIP simulations,
704 except for the more arid grass- and shrub-dominated sites. We note, however, that there are wide
705 differences in estimates for vegetation and soil carbon across the models, likely because of
706 different treatments of mortality and decomposition functions in these models.

Deleted: Fig.

Deleted: Fig.

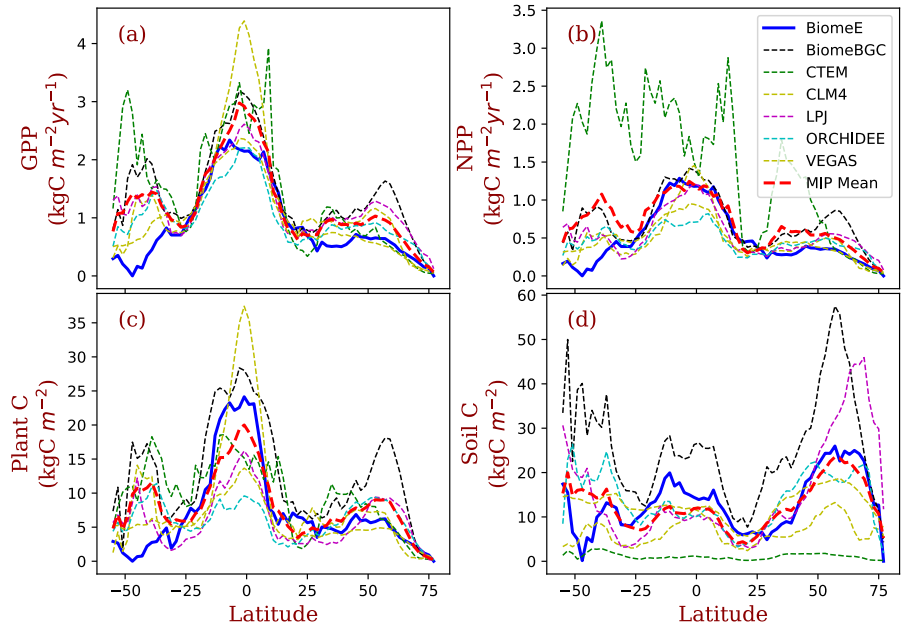

Figure 10 Latitudinal patterns of GPP, NPP, Biomass, and soil carbon as simulated by BiomeE (with full demography) and MsTMIP models. 'MIP Mean' is the mean of the six MsTMIP model simulations.

More broadly, the latitudinal mean of BiomeE simulated GPP is at the lower end of MsTMIP model predictions (Figure 10: a). Since BiomeE's GPP was tuned to fit remote sensing data derived GPP, the MsTMIP models may over-estimate global GPP. BiomeE simulated net primary production (NPP) (Figure 10: b), plant carbon (Figure 10: c), and soil carbon (Figure 10: d) are within the range simulated by the MsTMIP models. This indicates that BiomeE has slightly lower respiration than the MsTMIP models. In the arid regions (e.g., around latitude 40-50 °S), we simulated a lower GPP than that of MsTMIP models because of high drought sensitivity in our model.

Deleted:

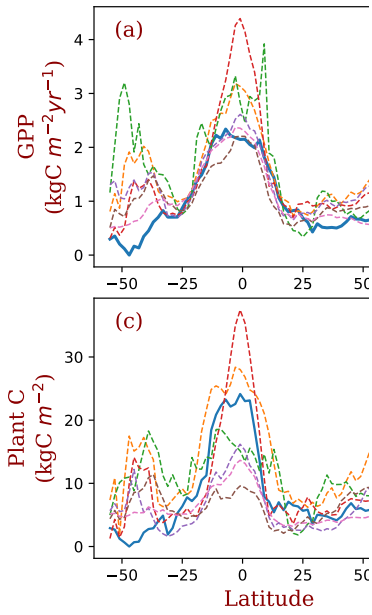

Formatted: Font: Not Bold

Deleted: Fig.

Deleted: Fig.

Deleted: Fig.

Deleted: Fig.

Deleted: our model's

Deleted: is lower

Deleted: 's

Deleted: sensitive

Deleted: responses

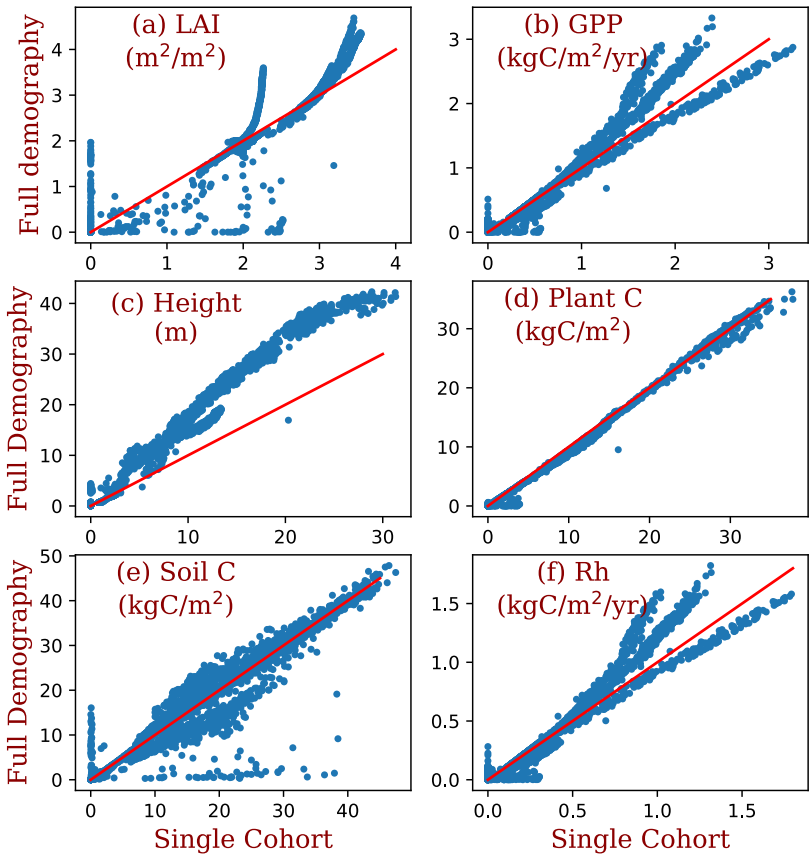

Figure 11 Comparison between the simulations of the full demography and the single cohort settings of BiomeE.

The demographic processes have significant impacts on the simulations of GPP, biomass, soil carbon, and vegetation structure compared to the single-cohort BiomeE (Figure 11). The full demographic BiomeE includes an understory layer of plants, resulting in higher LAI in high LAI regions and also slightly higher GPP. However, the total biomass predicted by the two model

Deleted: Higher GPP in the model with full demography leads to a high allocation to leaves and fine roots.

versions are similar because of the tradeoffs in allocation between leaves and stem growth and tree size distribution and because most biomass is in woody tissues (Please refer to the Figures S10 and S11 in the Supplementary Information for the single cohort BiomeE simulations). In the full demography model, tree mortality removes all the biomass, including leaves, fine roots, and stems, while in the single-cohort model, the mortality is represented as the turnover of woody biomass. Consequently, the full demography model has higher emergent turnover rate for the whole vegetation.

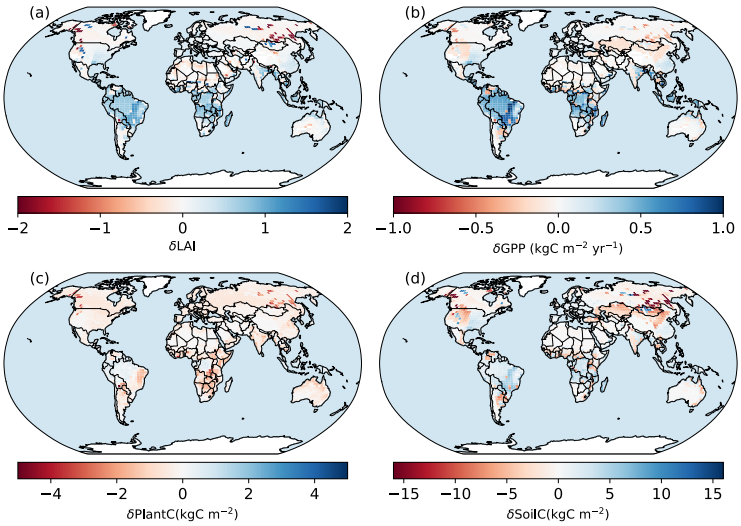

Figure 12 Spatial patterns of the differences between the simulations of the BiomeE: full demography minus the single-cohort simulations.

Compared to the single-cohort model, the full demography model predicts higher LAI and GPP in warm and wet regions and lower LAI and GPP in cold and dry regions (Figure 12: a, b). The full demography model also predicts much lower biomass and soil carbon than the single-cohort model in cold and dry regions (Figure 12: c). The reduced biomass input from full

Deleted: concentrated
Deleted: stems
Deleted: values
Deleted: Fig.
Deleted: Fig.
Deleted: Because the single cohort model has the same SOM pools and turnover/decomposition processes,
Deleted: t

demography alone is causing the difference in SOM dynamics since the two models share the same SOM pools and turnover/decomposition processes. Demographic processes greatly reduce model stability because reproduction and survival rates are low in dry and cold regions. By contrast, the single-cohort model does not simulate these processes explicitly and instead uses a simplified routine turnover of materials that allows plants to stay in extremely dry or cold conditions.

4.4 Eco-evolutionary simulation and sensitivity test

This model has the potential to predict competitively dominant PFTs in the continuum of plant traits through succession simulations according to the principles of evolutionarily optimal competition. We illustrate this with a set of simulations conducted at a series of ecosystem nitrogen content (from 269 to 575 g N/m^2) with five PFTs sampled from the continuums of LMA (σ, from 0.06 to 0.14) and target root/leaf area ratio (φ_{RL}, from 0.8 to 1.2 corresponding to each LMA). The differences in ecosystem total nitrogen represent the environmental conditions that can result from soil and climate conditions. The simulations were set as nitrogen-closed (i.e., no input and output of nitrogen). At the lowest ecosystem total nitrogen (Figure 13: a), the PFT with highest LMA (0.14 kg C/m^2 leaf) wins. With increases in ecosystem nitrogen (Figure 13: b - d), the winner shifts to lower LMA PFTs. This means that in infertile soils or cold climates with slower biogeochemical cycles (e.g., tundra and boreal forests), the eco-evolutionarily optimal PFTs should have high LMA leaves, and vice versa. This pattern is consistent with the predictions of a theoretical model derived in Weng et al. (2017). This simulation is also a case of the sensitivity test of vegetation dynamics at different environmental conditions. Vegetation can

Deleted: This is consistent with the functions of
Deleted: d
Deleted: in these regions, which
Deleted: er
Deleted: strategy
Deleted: t
Deleted: s
Deleted: are
Deleted: Fig.
Deleted: Fig.
Deleted: the simulated

shift their compositions and dominant plant traits to maintain an eco-evolutionarily optimal state, and thus amplify or attenuate the responses of ecosystem carbon cycle to climate changes.

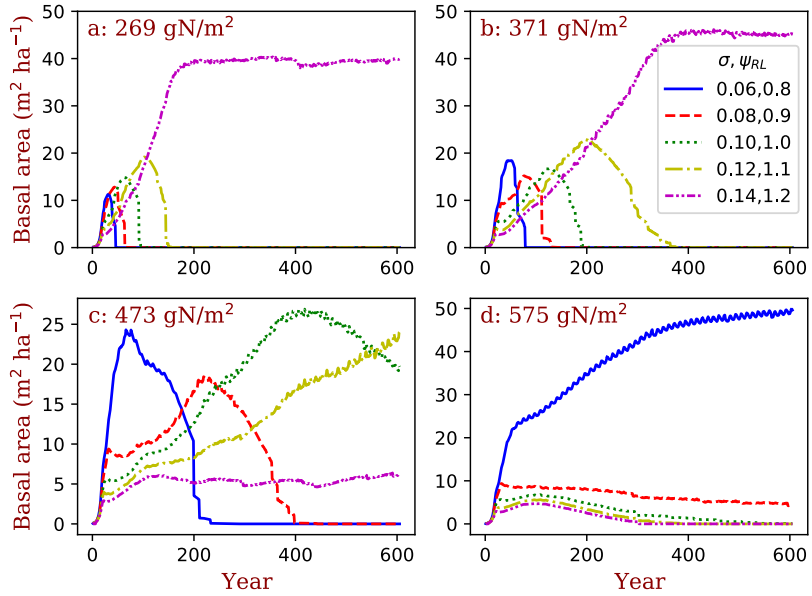

Figure 13. Simulated competitively dominant PFTs at different total ecosystem nitrogen. The simulations are set as nitrogen-closed (i.e., no input and output of nitrogen). The number in the title of each panel is the initial soil nitrogen. We used five PFTs that only differed in their LMA (σ) and target root/leaf area ratio (φ_{RL}) corresponding to each LMA in each simulation.

5 Discussion

We developed a parsimonious terrestrial ecosystem model for ModelE to simulate vegetation dynamics and ecosystem biogeochemical cycles. This model includes a cohort-based representation of vegetation structure, a height structured light competition scheme, demographic processes, and coupled carbon-nitrogen biogeochemical cycles. This model has four major

Formatted: Centered

811 modules that organize the hierarchical processes of ecosystems together into a cohesive
812 modeling structure: 1) plant physiology (photosynthesis, respiration), 2) plant phenology and
813 growth, 3) vegetation structural dynamics, and 4) soil biogeochemical cycles (Figure 1). Each
814 module is cohesive and has a minimum set of variables as the input from other modules.

815

816 **5.1 Model formulation**

817 In designing this model, we considered the simulation of competitively optimal strategy of plants
818 in different climates based on fundamental ecological rules (Purves and Pacala, 2008; Falster and
819 Westoby, 2003; Franklin et al., 2020). These strategies are mainly related to light competition,
820 water conditions, nutrient use efficiency, and disturbances (e.g., fire), and represented by the
821 traits of wood density, height growth, leaf longevity, and photosynthesis pathways. PFTs are
822 used in this model as an integrative unit representing combinations of plant traits for simulating
823 (1) the spontaneous dynamics of carbon, water, and energy fluxes as the core functions of an
824 ESM-based land model and (2) the transient vegetation structural and compositional dynamics
825 and ecosystem biogeochemical cycles in response to climate variations.

826 We adopted a generic design for the PFTs. Since the PFTs are samples of plant traits in
827 their natural ranges, the numbers of PFTs are flexible, depending on what strategies the users
828 wish to simulate (as the test simulations in Figure 13). This approach substantially simplifies the
829 parameterization of PFTs because it becomes selection of strategies in different trait values (i.e.,
830 parameters). Thus, the PFTs are adaptive and variable in different environmental conditions,
831 making it possible to reduce the number of PFTs while representing functional diversity and the
832 optimal adaptation to climate conditions.

Deleted: in the BiomeE

Deleted: test

Deleted: changes the parametrizations to the

Deleted: s

Deleted: through choosing

Deleted: can change to each other

Deleted: climate zones

To represent the major variations in plant functional diversity, we chose four plant traits as the primary axes to define PFTs: wood density, LMA, height growth parameter, and leaf maximum carboxylation rate. Wood density is relatively conservative (Swenson and Enquist, 2007; Chave et al., 2009), mostly ranging from 200 to 500 kg C m^{-3}, while herbaceous stem density ranges from 400~600 kg C m^{-3} (Niklas, 1995). However, herbaceous stems are usually hollow, making the ratio of total biomass to its volume low, and grasses shed their stems each growing season, resulting in faster stem turnover. It is a strategic difference from woody plants, which keep the woody tissues to build up their trunks and thus display their leaves on top of trunks for light competition (Dieckmann et al., 2007; Falster and Westoby, 2003). LMA is the key leaf trait that determines leaf life longevity and leaf types (i.e., evergreen vs. deciduous)) (Osnas et al., 2013), and represents the strategy for the competition in different soil nutrient levels (Tilman, 1988; Reich, 2014; Weng et al., 2017) and resistance to stresses of water and temperature (Oliveira et al., 2021).

The phenological type is simulated as an emergent property of plant physiological processes and strategies of dealing with seasonal air temperature and soil water variations. Three parameters – growing degree days, running mean daily temperature, and critical soil moisture – are used to define all possible phenological types. These three parameters are widely used in a variety of phenology models (e.g., Sitch et al., 2003; Prentice et al., 1992; Arora and Boer, 2005). However, phenology is not just a physiological response to the seasonality of climate conditions. Evergreen plants are distributed in periodically cold or dry climates. It is a competitively optimal strategy in infertile soil conditions (Aerts, 1995; Givnish, 2002; Coomes et al., 2005). The benefits and costs of keeping different leaves in cold or dry periods should be

Deleted: leaf mass per unit area (

Deleted:)

Deleted: (V_{cmax})

Deleted: In this model, t

Deleted: its

Deleted: y

Deleted: to

Deleted: variations of

Deleted:

Deleted: availability

Deleted: We used t

Deleted: (GDD)

realistically simulated based on eco-evolutionary theories for phenology modeling (e.g., Levine et al., 2022; Weng et al., 2017).

As for soil organic matter decomposition, the CASA model, which has 13 pools with different transfer coefficients and turnover rates (Randerson et al., 1997; Potter et al., 1993, 2003), is currently used in ModelE;. The soil biogeochemical cycle models developed thereafter have more sophisticated processes, especially those of microbial activities and carbon use efficiency (Manzoni et al., 2010; Wieder et al., 2014; Wang and Goll, 2021), and simplified carbon pools, mostly following CENTURY model structure (Parton et al., 1987). We chose an intermediate complexity scheme that has only two SOM pools but a functional microbial pool for decomposing SOM (Manzoni et al., 2010; Weng et al., 2017) so that the dynamics of SOM's C:N ratio, carbon use efficiency, and nitrogen mineralization can be reasonably simulated while keeping the model structure parsimonious.

5.2 Model predictions and performance

In this paper, we only evaluated the carbon cycle in the model simulations, though the nitrogen cycle is also simulated in tandem with the carbon cycle in the model. We did not extensively tune model parameters to fit observations because the purpose of this paper is to describe the formulation of the model. The core processes of this model, e.g., photosynthesis, respiration, phenology, growth, allocation, demography, soil biogeochemical cycles, are from well-developed models and have been shown able to capture observational patterns. Data assimilation approaches can be implemented when parameter tuning becomes essential (Luo et al., 2011; MacBean et al., 2016).

Deleted:

Deleted: is currently used in ModelE; it

Deleted: This model has four relatively distinctive sets of simulated variables that are critical for model performance and calibration: 1) Stomatal conductance, photosynthesis, and respiration; 2) demographic rates (i.e., allocation, structural growth, mortality, and reproduction); 3) LAI, tree size, crown self-organization, and vegetation structure; 4) Soil carbon and nitrogen storage.

Formatted: Indent: First line: 0.38"

The simulations demonstrate that this model can capture the global patterns of LAI, GPP, tree height, biomass, and soil carbon (Figure 7), even though the parameters are not extensively tuned. For example, global GPP patterns are consistent with those derived from SIF data (Figure7: c, d and Figure 8: b), and simulated tree heights span the same ranges of those derived from data. The simulated LAI is segregated by PFTs (Figure 8: a), largely because of the different parameter values of the maximum crown LAI for each PFT. The simulated biomass and soil carbon is generally higher than those of observations, though simulated soil carbon is lower in some cold regions.

Several factors likely explain the apparent discrepancies between simulated and observed LAI, GPP, biomass, and soil carbon in the model. First, the model uses a potential PFT distribution and does not account for land cover change and land use history. For example, carbon dense ecosystems (e.g., forests) have been extensively replaced by croplands and pastures. Second, while vegetation in the real world reflects a variety of successional stages and the effect of various disturbance events, our model analyses are based on equilibrium simulations without explicit disturbances, such as fire, deforestation and regrowth. Third, the model assumes mineral nitrogen is saturated and can consistently meet demands for plant growth. We did not fix the land cover mismatches by compromising ecosystem physiological processes because we cannot put all these effects into current model structure (i.e., mortality) when many processes are missing.

LAI is an illustrative variable for understanding why compromises are necessary when integrating ecological and demographic processes into an ESM. LAI, as a critical prognostic variable in vegetation models, links both plant physiology and biogeophysical interactions with climate systems (Richardson et al., 2012; Kelley et al., 2020; Park and Jeong, 2021). While LAI

Deleted: LAI,

Deleted: Fig.

Deleted: a

Deleted: b

Deleted: Fig.

Deleted: a

Deleted: in

Deleted: overestimates

Deleted: of

Deleted:

Deleted: ly based vegetation models

Deleted: s

is usually simulated by a fixed allocation scheme, even if the allocation ratios are dynamic with vegetation productivity or environmental conditions (Montané et al., 2017; Xia et al., 2019), the prediction of LAI is often simplified as the balance between leaf growth and turnover.

In practice, for ESMs, modelers tend to tune the LAI to fit observations and get the required albedo and water fluxes whatever the parameters of photosynthesis and respirations are. The uniform leaves within a crown would make the lower layer leaves have a negative carbon gain if the LAI was tuned close to that observed in tropical and boreal evergreen forests (around 5~7). Therefore, the photosynthesis rate must be tuned to fit the canopy photosynthesis by keeping these carbon negative leaves. The crown with carbon negative leaves do not affect the ecosystem carbon dynamics in the "single-cohort" models because the whole canopy net carbon gain can be tuned to fit the observations.

However, for the demographic models, the trees with different sizes are explicitly represented and placed in different layers. The vegetation community can create an understory condition where seedlings cannot survive because of light limitation and negative carbon gains (Weng et al., 2015). Since the leaf traits in the crown profile are functions of light, water and nitrogen (Niinemets et al., 2015), a more complex crown development module is required to simulate branching and leaf development and deployment processes. A tree should be able to optimize its LAI to maximize its fitness as a result of interactions among crown structure, light interception, and community-level competition (Anten, 2002; Niinemets and Anten, 2009; Hikosaka and Anten, 2012). For balancing the model complexity and computing efficiency, we defined a much small target LAI in this model to avoid carbon negative leaves.

The parameter V_{cmax} used in this model is also much lower than measured in young leaves (Bonan et al., 2011) because the aging of leaves is considered in the mean value of V_{cmax} of all

Deleted: in models

Deleted: M

Deleted: ir

Deleted: This LAI usually makes the lower layer leaves carbon negative. However, a first principle is that a tree should have an optimal LAI to maximize its carbon gain as a result of crown structure, light interception, and community-level competition(Anten, 2002; Hikosaka and Anten, 2012; Niinemets and Anten, 2009). Thus, in our model, because of the assumption of the uniform leaves within a crown, we defined a much small target LAI to avoid carbon negative leaves.…¶
¶
The "uniform leaf" assumption makes the lower layer leaves carbon negative when LAI is tuned close to that observed in tropical and boreal evergreen forests (where LAI is around 5~7). Therefore, the photosynthesis rate must be tuned to fit the canopy photosynthesis by keeping the carbon negative leaves. However, t

Deleted: ¶
The "uniform leaf" assumption makes the lower layer leaves carbon negative when LAI is tuned close to that obser... [2]

Deleted: is still reasonable and can be

Deleted: ted to

Deleted: observed dynamics

Deleted: This contrasts with

Deleted: version of the

Deleted: which represents

Deleted: and

Deleted: s

Deleted: s

Deleted: in the understory

Deleted: balances

Deleted: in some dry and cold regions

Deleted: T

Deleted: should, in reality,

Deleted: be

Deleted: a

Deleted: .

Deleted: A

Deleted: will then be

Deleted: Modelers should

Deleted: e

Deleted: then.

Deleted: leaf maximum carboxylation rate

Deleted: (

Deleted:)

leaves with different ages. The mean V_{cmax} of the whole canopy leaves is much lower than the new leaves that are usually used to measure V_{cmax}. If the leaves were not specifically chosen, the mean of measured V_{cmax} is much lower than those used in models as shown in Verryckt et al. (2022). This also indicates that V_{cmax} in current vegetation models is over-estimated.

In our model, the formulation of allometry makes the whole-tree's photosynthesis and respiration proportional to crown area, and thus the growth rate of tree diameter independent of crown area. The allocation scheme between the growth of stems and functional tissues (i.e., leaves and fine roots) is the strategy of resources foraging for light and soil resources, including height-structured competition for light. The vital rates drive vegetation structural changes and biogeochemical cycles (Purves et al., 2008). Our model makes it possible to simulate vegetation composition and structural dynamics based on the fundamental principles of ecology, and the transient changes in terrestrial ecosystems in response to climate change. This model therefore has the potential to predict competitively dominant strategies represented by plastic plant traits (e.g., competitively dominant LMA in the simulations of Figure 13), and the vegetation structure and composition that will be eco-evolutionarily optimized.

Deleted: The

Deleted: allometry of plant architecture, rules for plant growth, and reproduction and mortality processes form the basis of vegetation structural dynamics.

Deleted: T

Deleted: Fig.

5.3 Major uncertainties in BiomeE

Global vegetation models typically require simplifying assumptions to organize ecosystem processes at different scales into a cohesive model structure that balances the complexity of ecosystem processes and the limitations of our knowledge (Prentice et al., 1992, 2007; Harrison et al., 2021). In our model, many processes, including phenology and drought effects, are based on phenomenological equations representing the poorly understood links between processes needed by the model to simulate the entire system. In the following sections,

we highlight these assumptions and evaluate their relative benefits and costs. Transparency in the description of a community model such as this one will help future developers understand model compromises and the processes that should be improved. The following phenomenological relationships represent the major sources of uncertainty in this model.

Water limitation of photosynthesis is calculated as a function of relative soil moisture following the water stress function from Rodriguez-Iturbe et al. (1999):

$$\beta_D = Min\left(1.0, max\left(\frac{s_D - s_{min}}{s^* - s_{min}}, 0.0\right)\right), \quad (16)$$

The parameters s^* and $s_{\min}$ are PFT-specific, representing different responses of PFTs to soil water conditions, and S_D is the relative soil moisture ranging from 0 (soil water content at wilting point) to 1 (at field capacity). This formulation that scales soil moisture to a scalar between zero to 1 is repeatedly used in both physiological responses of photosynthesis and phenology in ecosystem models as a simplistic treatment of the central role of water limitation on plant physiology (Powell et al., 2013; De Kauwe et al., 2015; Harper et al., 2021). This equation does not include the detailed processes of plant hydraulics and its adaptation to arid environments.

Plants have multiple tradeoffs and strategies to improve their competitiveness under water stress, such as regulating stomata conductance, shedding leaves, producing more roots, etc. (Oliveira et al., 2021; Volaire, 2018). At the ecosystem level, competition and evolutionary processes filter community emergent properties (Franklin et al., 2020; van der Molen et al., 2011). For example, trees in different climate regions have similar hydraulic safety margins (Choat et al., 2012), partly due to the intense competition for light (height growth) and water (root allocation) that require optimal use of available resources at any climate conditions (Gleason et al., 2017; Liu et al., 2019). However, in this model, the drought responses are only

Deleted: areas
Deleted: can
Deleted: with new information or approaches

delineated by Eq. 16. The parameter choices for s^* and s_{min} likely explain the amplified water stresses and low productivity in arid regions within our model.

Phenology represents the seasonal rhythms of plant physiological activities as adapted to periodic changes in temperature, precipitation, and light availability (Abramoff and Finzi, 2015; Caldararu et al., 2014; Chuine, 2010). DGVMs normally simulate leaf onset and senescence based on temperature conditions for cold deciduous plants and soil water conditions for drought deciduous plants (Arora and Boer, 2005; Caldararu et al., 2014). Phenology modeling is still highly empirical, although new models and approaches for cold deciduous and drought deciduous strategies have been proposed recently (e.g., Caldararu et al., 2014; Dahlin et al., 2015; Manzoni et al., 2015; Chen et al., 2016). We used a simple formulation of temperature and drought responses (Eqs. 1 and 3). For the cold-deciduous strategies, the phenology model balances growing season length and frost risks by adjusting critical GDD0 and T0 according to chilling days and growing days to reduce frost risk in warm regions and increase growing season length in cold regions. In this way, leaf senescence also considers growing season length and leaf aging. For example, in areas with longer growing seasons, plants will have a higher T0 and initiate senescence at higher temperatures. For the drought phenology, we set different critical soil moisture indexes to initiate and terminate a growing season (Table 1). However, these relationships are phenomenological, and ecological rules will benefit future model development.

Mortality is an integrative process of accumulative physiological stresses, structural damages, and disturbances in a tree's lifetime. The direct causes can be starvation, structural failure, hydraulic failure, etc. (McDowell, 2011; Aakala et al., 2012; Aleixo et al., 2019). We only consider the background mortality and define its rate as a function of tree diameter and light

Deleted: (Eqs 1 and 3)

Deleted: result

Deleted: during

Deleted: reasons

Deleted: In this model,

Deleted: w

environment (Eq. 10). Hydraulic failure-induced mortality is required for realistically modeling plant responses to climate changes.

We employed these general phenomenological equations primarily because more mechanistic equations are not currently known. We are using the key variables that characterize ecosystem properties to define the basic model structure but have to use less-than-solid information to link them together by phenomenological relationships, as all the models do. In addition, our interest is to keep this model as simple as possible to improve interpretability and transparency and to reduce the computational burden when it is integrated into the ModelE. In these places where the tradeoff between model complexity and process accuracy is necessary, we highlight the underlying assumptions clearly, rather than implementing temporary fixes that lack solid ecological principles.

5.4 Insights from comparison with MsTMIP model

Most of the MsTMIP participant models have been analyzed by a model traceability method developed by Xia et al. (2013), which hierarchically decomposes model behavior into some fundamental processes of ecosystem carbon dynamics, such as GPP, carbon use efficiency (CUE), allocation coefficients, carbon residence time, carbon storage capacity, and environmental response functions (Xia et al., 2013; Cui et al., 2019; Zhou et al., 2021). This method is based on the assumptions of the linear system and the ecosystem emergent behavior per se (Eriksson, 1971; Emanuel and Killough, 1984; Luo et al., 2012; Sierra et al., 2018), making it is consistent with the concepts that are used as the basis of ecosystem carbon cycle models. The analyses of model traceability found, for the carbon cycle dynamics, the major uncertainty is from the modeling of the turnover rates (reciprocals of residence time) of

Deleted: studying

Formatted: Line spacing: Double

vegetation and soil carbon pools (Chen et al., 2015; Jiang et al., 2017). From CMIP5 to CMIP6, the modeling of NPP has been greatly improved, while the ecosystem carbon residence time remains highly biased (Wei et al., 2022).

According to the concepts of this traceability analysis approach (Xia et al., 2013), BiomeE also has a high uncertainty in the modeling of residence times of vegetation and soil carbon pools, because the mortality is picked up from the global forest data and the SOC decomposition processes are highly simplified. These issues have been discussed in the section of "5.3 Major uncertainties in BiomeE". These concepts (e.g., residence time, allocation coefficients) describe model emergent properties resulting from the underlying biological and ecological processes (i.e., micro-dynamics vs. macro-states). Fitting the emergent properties directly to improve model behavior is natural and convenient because many vegetation models are using these emergent properties (e.g., CUE, residence time, and allocation coefficients) to describe ecosystem processes in their formulations as a tradition of ecosystem modeling.

There are a couple of common and long-lasting issues in terrestrial ecosystem modeling, such as responses to warming, responses to atmospheric CO_2, drought stress effects, and vegetation compositional changes (Luo, 2007; Franklin et al., 2020; Harrison et al., 2021). These issues represent our knowledge gaps in ecosystem ecology. For modeling vegetation dynamics eco-evolutionarily, we need to use the fundamental ecological processes and unbreakable physical rules to simulate the emergent processes (e.g., Scheiter et al., 2013; Weng et al., 2019), With the design of vegetation modeling in the BiomeE, such as the explicit demographic processes, individual-based competition for different resources, and flexible trait combinations of PFTs, this model is able to predict some key emergent dynamics of ecosystems based on the underlying biological and evolutionary mechanisms (as shown in Figure 13). Data from field

experiments (Ainsworth and Long, 2004; Crowther et al., 2016), observatory networks (e.g., Fluxnet, Baldocchi et al., 2001; Friend et al., 2007), and remote sensing (Duncanson et al., 2020), can provide direct information for modeling the underlying ecological processes and validating predicted emergent properties.

5.5 Model stability and complexity

Ecosystem demographic processes (e.g., reproduction and mortality) are a source of high sensitivity and uncertainty in BiomeE. In some environmental conditions, especially in dry or cold regions, the predefined parameters can lead to high mortality or failure of reproduction, making ecosystems highly instable. To understand these issues, we developed a "single-cohort" version of the model to aid in the diagnosis of issues in the full demographic version of the model. The major issue we identified is the fact that the model formulation is based on functional processes in highly-productive regions, whereas the model is applied globally and across much more diverse environmental conditions (e.g., arid environments). The variables and parameters that work well in highly-productive regions (e.g., initial seedling sizes, default leaf growth, minimum allocation ratios, etc.) are often unsuitable in regions with higher environmental stress. And although plants have evolved special features to deal with more extreme conditions (Lloret et al., 2012; Reyer et al., 2013; Singh et al., 2020), these features have not yet been integrated into the model.

There is a tendency in current DGVMs to use individual plant physiological trait changes to represent community shifts. This approach is usually characterized as "parameter dynamics" or "response functions" (Fisher and Koven, 2020; Luo and Schuur, 2020) for reducing model processes and complexity. Adding new processes to work around existing problems, instead of

redesigning the fundamental model processes, is common in model development. The approach is helpful for tracking model development, undoing wrong additions, and improving model performance. However, work-arounds often increase model complexity without concomitant improvements in model predictions.

Generally, a model's usefulness is improved by transparent assumptions, a well-defined model structure, and output that is testable against data (Famiglietti et al., 2021; Forster, 2017; Hourdin et al., 2017). Data assimilation approaches improve model parameterization more efficiently and effectively than manually tuning individual parameters (Wang et al., 2009; Williams et al., 2009; MacBean et al., 2016) and allow for more detailed uncertainty analysis (Luo et al., 2009; Weng et al., 2011; Weng and Luo, 2011; Xu et al., 2006; Dietze, 2014). It is important to only include necessary assumptions in a model and to include them in ways that do not compromise other processes or parameters. Modelers should try their best not to add poor-understood processes if not necessary. Additionally, many specifications of model formulation are based on the questions that a user is trying to answer in their research. We should not expect to develop an all-encompassing model that fits all application scenarios. On the contrary, maintaining model flexibility and transparency is critical for using this model as a tool to explore specific science questions. In BiomeE, we have opted for what we consider the most parsimonious and, at the same time, theoretically sound formulations of allometry, phenology, and allocation dynamics to allow for computational efficiency in capturing vegetation grown and ecological dynamics in the context of an ESM.

5.6 Legacy limitations of ModelE coding and development conventions

The legacy of model coding structure and the history of model development can greatly affect the functions and the selection of model formulations (Alexander and Easterbrook, 2015). ModelE was developed as a general circulation model, and vegetation in the model to date has been represented with a simple set of static biophysics parameterizations to regulate exchanges of energy and moisture between the land surface and the atmosphere (Hansen et al., 2007; Schmidt et al., 2014; Kelley et al., 2020). To advance the functionality of the vegetation and the land surface model within ModelE, increases in complexity must therefore be balanced with the computational demands of a fully coupled model.

In ModelE, the land model, TerraE, is used to calculate land surface (including vegetation) water and energy fluxes and soil water dynamics based on the characteristics of vegetation derived from the vegetation model (e.g., canopy conductance, wetness, etc.) at the grid scale. It does not calculate each cohort's transpiration and water uptake. In BiomeE, the water limitation of stomatal conductance is calculated as a function of soil water stress index and root vertical distribution, instead of the direct plant root water supply (plant hydraulics). This setting works well for the big leaf model (one canopy at one grid). However, when multiple cohorts of plants are represented, as we do in BiomeE, it is unable to represent water competition and differentiate the contribution of each single cohort's contribution to the total transpiration. A structural change will be required to solve this problem by calculating transpiration from the bottom-up (i.e., from cohort up to grid cell).

Deleted: the

Deleted: fully-coupled

Deleted: our vegetation model

6 Conclusions

We developed a new demographic vegetation model to improve the representation of terrestrial vegetation dynamics and ecosystem biogeochemical cycles in the NASA Goddard Institute of

Space Studies' coupled Earth system model, ModelE. This model includes the processes of plant growth, mortality, reproduction, vegetation structural dynamics, and soil carbon and nitrogen cycling. To scale this model globally, we added a new set of plant functional types to represent global vegetation functional diversity and introduced new phenology algorithms to deal with the seasonality of temperature and soil water availability. Competition for light and soil resources is individual-based, which makes the modeling of eco-evolutionary optimality possible. This model predicts the dynamics of vegetation and soil biogeochemistry including leaf area index, vegetation structure (e.g., height, tree density, size distribution, crown organization), and ecosystem carbon and nitrogen storage and fluxes. This model will enable ModelE to simulate long-term biogeophysical and biogeochemical feedbacks between the climate system and land ecosystems at decadal to century temporal scales. It will also allow for the prediction of transient vegetation dynamics and eco-evolutionary community assemblage in response to future climate changes based on the fundamental ecological principles.

Code and data availability

The model codes have been coupled with NASA GISS ModelE and will be released with ModelE codes (https://www.giss.nasa.gov/tools/modelE/). The codes of BiomeE module are available at https://doi.org/10.5281/zenodo.6476152. The simulated data have been archived at Zenodo (https://doi.org/10.5281/zenodo.6480411).

Author contributions

EW coded the model and performed test runs and data analysis. EW and BIC wrote the first draft of the manuscript. BIC, MJP, SSM, NYK, and EW designed the functional coupling with ModelE and the land module. NYK, IA, RS, and MK contributed to input data, the IO structure and the coupling between BiomeE and ModelE. KW, RD, CE, and SWP contributed to conceptual model development and PFT design. All co-authors contributed to writing or improving the manuscript.

Competing interests

The authors declare that they have no conflict of interest.

Acknowledgements

This work was supported by NASA Modeling, Analysis, and Prediction (MAP) Program (award numbers: 80NSSC21K1496, NNH10ZDA001N, and 16-MAP16-0149). Computing resources for the model runs were provided by the NASA High-End Computing (HEC) Program through the NASA Center for Climate Simulation (NCCS) at Goddard Space Flight Center. We thank Dr. Pierre Gentine of Department of Earth and Environmental Engineering, Columbia University, for his help in GPP data and model validation, and Dr. Anastasia Romanou of NASA Goddard Institute of Space Studies for discussions in ModelE codes structure.

Reference

Aakala, T., Fraver, S., Palik, B. J., and D'Amato, A. W.: Spatially random mortality in old-growth red pine forests of northern Minnesota, Canadian Journal of Forest Research, 42, 899–907, https://doi.org/10.1139/x2012-044, 2012.

Abramoff, R. Z. and Finzi, A. C.: Are above- and below-ground phenology in sync?, New Phytologist, 205, 1054–1061, https://doi.org/10.1111/nph.13111, 2015.

Aerts, R.: The advantages of being evergreen, Trends in Ecology & Evolution, 10, 402–407, https://doi.org/10.1016/S0169-5347(00)89156-9, 1995.

Ainsworth, E. A. and Long, S. P.: What have we learned from 15 years of free-air CO2 enrichment (FACE)? A meta-analytic review of the responses of photosynthesis, canopy properties and plant production to rising CO2: Tansley review, New Phytologist, 165, 351–372, https://doi.org/10.1111/j.1469-8137.2004.01224.x, 2004.

Aleixo, I., Norris, D., Hemerik, L., Barbosa, A., Prata, E., Costa, F., and Poorter, L.: Amazonian rainforest tree mortality driven by climate and functional traits, Nature Climate Change, 9, 384–388, https://doi.org/10.1038/s41558-019-0458-0, 2019.

Alemohammad, S. H., Fang, B., Konings, A. G., Aires, F., Green, J. K., Kolassa, J., Miralles, D., Prigent, C., and Gentine, P.: Water, Energy, and Carbon with Artificial Neural Networks (WECANN): a statistically based estimate of global surface turbulent fluxes and gross primary productivity using solar-induced fluorescence, Biogeosciences, 14, 4101–4124, https://doi.org/10.5194/bg-14-4101-2017, 2017.

Alexander, K. and Easterbrook, S. M.: The software architecture of climate models: a graphical comparison of CMIP5 and EMICAR5 configurations, Geoscientific Model Development, 8, 1221–1232, https://doi.org/10.5194/gmd-8-1221-2015, 2015.

Allen, C. D., Macalady, A. K., Chenchouni, H., Bachelet, D., McDowell, N., Vennetier, M., Kitzberger, T., Rigling, A., Breshears, D. D., Hogg, E. H. (Ted), Gonzalez, P., Fensham, R., Zhang, Z., Castro, J., Demidova, N., Lim, J.-H., Allard, G., Running, S. W., Semerci, A., and Cobb, N.: A global overview of drought and heat-induced tree mortality reveals emerging climate change risks for forests, Forest Ecology and Management, 259, 660–684, https://doi.org/10.1016/j.foreco.2009.09.001, 2010.

Anderegg, W. R. L., Kane, J. M., and Anderegg, L. D. L.: Consequences of widespread tree mortality triggered by drought and temperature stress, Nature Climate Change, 3, 30–36, https://doi.org/10.1038/nclimate1635, 2012.

Anten, N. P.: Evolutionarily stable leaf area production in plant populations, Journal of Theoretical Biology, 217, 15–32, 2002.

Argles, A. P. K., Moore, J. R., Huntingford, C., Wiltshire, A. J., Harper, A. B., Jones, C. D., and Cox, P. M.: Robust Ecosystem Demography (RED version 1.0): a parsimonious approach to

modelling vegetation dynamics in Earth system models, Geoscientific Model Development, 13, 4067–4089, https://doi.org/10.5194/gmd-13-4067-2020, 2020.

Arora, V. K. and Boer, G. J.: A parameterization of leaf phenology for the terrestrial ecosystem component of climate models, Global Change Biology, 11, 39–59, https://doi.org/10.1111/j.1365-2486.2004.00890.x, 2005.

Arora, V. K., Katavouta, A., Williams, R. G., Jones, C. D., Brovkin, V., Friedlingstein, P., Schwinger, J., Bopp, L., Boucher, O., Cadule, P., Chamberlain, M. A., Christian, J. R., Delire, C., Fisher, R. A., Hajima, T., Ilyina, T., Joetzjer, E., Kawamiya, M., Koven, C. D., Krasting, J. P., Law, R. M., Lawrence, D. M., Lenton, A., Lindsay, K., Pongratz, J., Raddatz, T., Séférian, R., Tachiiri, K., Tjiputra, J. F., Wiltshire, A., Wu, T., and Ziehn, T.: Carbon–concentration and carbon–climate feedbacks in CMIP6 models and their comparison to CMIP5 models, Biogeosciences, 17, 4173–4222, https://doi.org/10.5194/bg-17-4173-2020, 2020.

Avissar, R. and Werth, D.: Global Hydroclimatological Teleconnections Resulting from Tropical Deforestation, J. Hydrometeor., 6, 134–145, https://doi.org/10.1175/JHM406.1, 2005.

Baldocchi, D., Falge, E., Gu, L., Olson, R., Hollinger, D., Running, S., Anthoni, P., Bernhofer, C., Davis, K., Evans, R., Fuentes, J., Goldstein, A., Katul, G., Law, B., Lee, X., Malhi, Y., Meyers, T., Munger, W., Oechel, W., Paw U, K. T., Pilegaard, K., Schmid, H. P., Valentini, R., Verma, S., Vesala, T., Wilson, K., and Wofsy, S.: FLUXNET: A New Tool to Study the Temporal and Spatial Variability of Ecosystem-Scale Carbon Dioxide, Water Vapor, and Energy Flux Densities, Bull. Amer. Meteor. Soc., 82, 2415–2434, https://doi.org/10.1175/1520-0477(2001)082<2415:FANTTS>2.3.CO;2, 2001.

Beer: Bestimmung der Absorption des rothen Lichts in farbigen Flüssigkeiten, Annalen der Physik, 162, 78–88, https://doi.org/10.1002/andp.18521620505, 1852.

Berzaghi, F., Wright, I. J., Kramer, K., Oddou-Muratorio, S., Bohn, F. J., Reyer, C. P. O., Sabaté, S., Sanders, T. G. M., and Hartig, F.: Towards a New Generation of Trait-Flexible Vegetation Models, Trends in Ecology & Evolution, https://doi.org/10.1016/j.tree.2019.11.006, 2019.

Bonan, G. B., Lawrence, P. J., Oleson, K. W., Levis, S., Jung, M., Reichstein, M., Lawrence, D. M., and Swenson, S. C.: Improving canopy processes in the Community Land Model version 4 (CLM4) using global flux fields empirically inferred from FLUXNET data, Journal of Geophysical Research, 116, https://doi.org/10.1029/2010JG001593, 2011.

Brando, P. M., Paolucci, L., Ummenhofer, C. C., Ordway, E. M., Hartmann, H., Cattau, M. E., Rattis, L., Medjibe, V., Coe, M. T., and Balch, J.: Droughts, Wildfires, and Forest Carbon Cycling: A Pantropical Synthesis, Annu. Rev. Earth Planet. Sci., 47, 555–581, https://doi.org/10.1146/annurev-earth-082517-010235, 2019.

Briones, M. J. I., McNamara, N. P., Poskitt, J., Crow, S. E., and Ostle, N. J.: Interactive biotic and abiotic regulators of soil carbon cycling: evidence from controlled climate experiments on peatland and boreal soils, GLOBAL CHANGE BIOLOGY, 20, 2971–2982, https://doi.org/10.1111/gcb.12585, 2014.

Brodribb, T. J., Powers, J., Cochard, H., and Choat, B.: Hanging by a thread? Forests and drought, Science, 368, 261–266, https://doi.org/10.1126/science.aat7631, 2020.

Caldararu, S., Purves, D. W., and Palmer, P. I.: Phenology as a strategy for carbon optimality: a global model, Biogeosciences, 11, 763–778, https://doi.org/10.5194/bg-11-763-2014, 2014.

Chave, J., Coomes, D., Jansen, S., Lewis, S. L., Swenson, N. G., and Zanne, A. E.: Towards a worldwide wood economics spectrum, Ecology Letters, 12, 351–366, https://doi.org/10.1111/j.1461-0248.2009.01285.x, 2009.

Chen, M., Melaas, E. K., Gray, J. M., Friedl, M. A., and Richardson, A. D.: A new seasonal-deciduous spring phenology submodel in the Community Land Model 4.5: impacts on carbon and water cycling under future climate scenarios, Global Change Biology, 22, 3675–3688, https://doi.org/10.1111/gcb.13326, 2016.

Chen, Y., Xia, J., Sun, Z., Li, J., Luo, Y., Gang, C., and Wang, Z.: The role of residence time in diagnostic models of global carbon storage capacity: model decomposition based on a traceable scheme, Sci Rep, 5, 16155, https://doi.org/10.1038/srep16155, 2015.

Choat, B., Jansen, S., Brodribb, T. J., Cochard, H., Delzon, S., Bhaskar, R., Bucci, S. J., Feild, T. S., Gleason, S. M., Hacke, U. G., Jacobsen, A. L., Lens, F., Maherali, H., Martínez-Vilalta, J., Mayr, S., Mencuccini, M., Mitchell, P. J., Nardini, A., Pittermann, J., Pratt, R. B., Sperry, J. S., Westoby, M., Wright, I. J., and Zanne, A. E.: Global convergence in the vulnerability of forests to drought, Nature, https://doi.org/10.1038/nature11688, 2012.

Chuine, I.: Why does phenology drive species distribution?, Philosophical Transactions of the Royal Society B: Biological Sciences, 365, 3149–3160, https://doi.org/10.1098/rstb.2010.0142, 2010.

Clark, J. S., Iverson, L., Woodall, C. W., Allen, C. D., Bell, D. M., Bragg, D. C., D'Amato, A. W., Davis, F. W., Hersh, M. H., Ibanez, I., Jackson, S. T., Matthews, S., Pederson, N., Peters, M., Schwartz, M. W., Waring, K. M., and Zimmermann, N. E.: The impacts of increasing drought on forest dynamics, structure, and biodiversity in the United States, Global Change Biology, 22, 2329–2352, https://doi.org/10.1111/gcb.13160, 2016.

Coomes, D. A., Allen, R. B., Bentley, W. A., Burrows, L. E., Canham, C. D., Fagan, L., Forsyth, D. M., Gaxiola-Alcantar, A., Parfitt, R. L., Ruscoe, W. A., Wardle, D. A., Wilson, D. J., and Wright, E. F.: The hare, the tortoise and the crocodile: the ecology of angiosperm dominance, conifer persistence and fern filtering, Journal of Ecology, 93, 918–935, https://doi.org/10.1111/j.1365-2745.2005.01012.x, 2005.

Crowther, T. W., Todd-Brown, K. E. O., Rowe, C. W., Wieder, W. R., Carey, J. C., Machmuller, M. B., Snoek, B. L., Fang, S., Zhou, G., Allison, S. D., Blair, J. M., Bridgham, S. D., Burton, A. J., Carrillo, Y., Reich, P. B., Clark, J. S., Classen, A. T., Dijkstra, F. A., Elberling, B., Emmett, B. A., Estiarte, M., Frey, S. D., Guo, J., Harte, J., Jiang, L., Johnson, B. R., Kröel-Dulay, G., Larsen, K. S., Laudon, H., Lavallee, J. M., Luo, Y., Lupascu, M., Ma, L. N., Marhan, S., Michelsen, A., Mohan, J., Niu, S., Pendall, E., Peñuelas, J., Pfeifer-Meister, L., Poll, C., Reinsch, S., Reynolds, L. L., Schmidt, I. K., Sistla, S., Sokol, N. W., Templer, P. H., Treseder, K. K.,

Welker, J. M., and Bradford, M. A.: Quantifying global soil carbon losses in response to warming, Nature, 540, 104–108, https://doi.org/10.1038/nature20150, 2016.

Cui, E., Huang, K., Arain, M. A., Fisher, J. B., Huntzinger, D. N., Ito, A., Luo, Y., Jain, A. K., Mao, J., Michalak, A. M., Niu, S., Parazoo, N. C., Peng, C., Peng, S., Poulter, B., Ricciuto, D. M., Schaefer, K. M., Schwalm, C. R., Shi, X., Tian, H., Wang, W., Wang, J., Wei, Y., Yan, E., Yan, L., Zeng, N., Zhu, Q., and Xia, J.: Vegetation Functional Properties Determine Uncertainty of Simulated Ecosystem Productivity: A Traceability Analysis in the East Asian Monsoon Region, Global Biogeochemical Cycles, 33, 668–689, https://doi.org/10.1029/2018GB005909, 2019.

Dahlin, K. M., Fisher, R. A., and Lawrence, P. J.: Environmental drivers of drought deciduous phenology in the Community Land Model, Biogeosciences, 12, 5061–5074, https://doi.org/10.5194/bg-12-5061-2015, 2015.

Davidson, E. A. and Janssens, I. A.: Temperature sensitivity of soil carbon decomposition and feedbacks to climate change, Nature, 440, 165–173, https://doi.org/10.1038/nature04514, 2006.

De Kauwe, M. G., Zhou, S.-X., Medlyn, B. E., Pitman, A. J., Wang, Y.-P., Duursma, R. A., and Prentice, I. C.: Do land surface models need to include differential plant species responses to drought? Examining model predictions across a mesic-xeric gradient in Europe, Biogeosciences, 12, 7503–7518, https://doi.org/10.5194/bg-12-7503-2015, 2015.

Dieckmann, U., Brannstrom, A., HilleRisLambes, R., and Ito, H. C.: The Adaptive Dynamics of Community Structure, in: Mathematics for Ecology and Environmental Sciences, edited by: Takeuchi, Yasuhiro, Iwasa, Yoh, and Sato, Kazunori, Springer, 145–177, 2007.

Dietze, M. C.: Gaps in knowledge and data driving uncertainty in models of photosynthesis, PHOTOSYNTHESIS RESEARCH, 119, 3–14, https://doi.org/10.1007/s11120-013-9836-z, 2014.

Duncanson, L., Neuenschwander, A., Hancock, S., Thomas, N., Fatoyinbo, T., Simard, M., Silva, C. A., Armston, J., Luthcke, S. B., Hofton, M., Kellner, J. R., and Dubayah, R.: Biomass estimation from simulated GEDI, ICESat-2 and NISAR across environmental gradients in Sonoma County, California, Remote Sensing of Environment, 242, 111779, https://doi.org/10.1016/j.rse.2020.111779, 2020.

Dybzinski, R., Farrior, C., Wolf, A., Reich, P. B., and Pacala, S. W.: Evolutionarily Stable Strategy Carbon Allocation to Foliage, Wood, and Fine Roots in Trees Competing for Light and Nitrogen: An Analytically Tractable, Individual-Based Model and Quantitative Comparisons to Data, American Naturalist, 177, 153–166, https://doi.org/10.1086/657992, 2011.

Dybzinski, R., Farrior, C. E., and Pacala, S. W.: Increased forest carbon storage with increased atmospheric CO2 despite nitrogen limitation: a game-theoretic allocation model for trees in competition for nitrogen and light, Global Change Biology, 21, 1182–1196, https://doi.org/10.1111/gcb.12783, 2015.

Emanuel, W. R. and Killough, G. G.: Modeling terrestrial ecosystems in the global carbon cycle with Shifts in carbon storage capacity by land-use change, Ecology, 65, 970–983, https://doi.org/10.2307/1938069, 1984.

Eriksson, E.: Compartment Models and Reservoir Theory, Annual Review of Ecology and Systematics, 2, 67–84, https://doi.org/10.1146/annurev.es.02.110171.000435, 1971.

Euskirchen, E. S., Edgar, C. W., Turetsky, M. R., Waldrop, M. P., and Harden, J. W.: Differential response of carbon fluxes to climate in three peatland ecosystems that vary in the presence and stability of permafrost, Journal of Geophysical Research: Biogeosciences, 119, 1576–1595, https://doi.org/10.1002/2014JG002683, 2014.

Falster, D. and Westoby, M.: Plant height and evolutionary games, Trends in Ecology & Evolution, 18, 337–343, https://doi.org/10.1016/S0169-5347(03)00061-2, 2003.

Falster, D. S., FitzJohn, R. G., Brannstrom, A., Dieckmann, U., and Westoby, M.: plant: A package for modelling forest trait ecology and evolution, METHODS IN ECOLOGY AND EVOLUTION, 7, 136–146, https://doi.org/10.1111/2041-210X.12525, 2016.

Falster, D. S., Braennstroem, A., Westoby, M., and Dieckmann, U.: Multitrait successional forest dynamics enable diverse competitive coexistence, PROCEEDINGS OF THE NATIONAL ACADEMY OF SCIENCES OF THE UNITED STATES OF AMERICA, 114, E2719–E2728, https://doi.org/10.1073/pnas.1610206114, 2017.

Famiglietti, C. A., Smallman, T. L., Levine, P. A., Flack-Prain, S., Quetin, G. R., Meyer, V., Parazoo, N. C., Stettz, S. G., Yang, Y., Bonal, D., Bloom, A. A., Williams, M., and Konings, A. G.: Optimal model complexity for terrestrial carbon cycle prediction, Biogeosciences, 18, 2727–2754, https://doi.org/10.5194/bg-18-2727-2021, 2021.

Farrior, C. E.: Theory predicts plants grow roots to compete with only their closest neighbours, Proceedings of the Royal Society B: Biological Sciences, 286, 20191129, https://doi.org/10.1098/rspb.2019.1129, 2019.

Farrior, C. E., Dybzinski, R., Levin, S. A., and Pacala, S. W.: Competition for Water and Light in Closed-Canopy Forests: A Tractable Model of Carbon Allocation with Implications for Carbon Sinks, American Naturalist, 181, 314–330, https://doi.org/10.1086/669153, 2013.

Fisher, R. A. and Koven, C. D.: Perspectives on the Future of Land Surface Models and the Challenges of Representing Complex Terrestrial Systems, Journal of Advances in Modeling Earth Systems, 12, e2018MS001453, https://doi.org/10.1029/2018MS001453, 2020.

Fisher, R. A., Muszala, S., Verteinstein, M., Lawrence, P., Xu, C., McDowell, N. G., Knox, R. G., Koven, C., Holm, J., Rogers, B. M., Spessa, A., Lawrence, D., and Bonan, G.: Taking off the training wheels: the properties of a dynamic vegetation model without climate envelopes, CLM4.5(ED), GEOSCIENTIFIC MODEL DEVELOPMENT, 8, 3593–3619, https://doi.org/10.5194/gmd-8-3593-2015, 2015.

Forster, P.: Half a century of robust climate models, Nature, 545, 296–297, https://doi.org/10.1038/545296a, 2017.

Franklin, O., Johansson, J., Dewar, R. C., Dieckmann, U., McMurtrie, R. E., Brannstrom, A., and Dybzinski, R.: Modeling carbon allocation in trees: a search for principles, Tree Physiology, 32, 648–666, https://doi.org/10.1093/treephys/tpr138, 2012.

Franklin, O., Harrison, S. P., Dewar, R., Farrior, C. E., Brännström, Å., Dieckmann, U., Pietsch, S., Falster, D., Cramer, W., Loreau, M., Wang, H., Mäkelä, A., Rebel, K. T., Meron, E., Schymanski, S. J., Rovenskaya, E., Stocker, B. D., Zaehle, S., Manzoni, S., van Oijen, M., Wright, I. J., Ciais, P., van Bodegom, P. M., Peñuelas, J., Hofhansl, F., Terrer, C., Soudzilovskaia, N. A., Midgley, G., and Prentice, I. C.: Organizing principles for vegetation dynamics, Nature Plants, 1–10, https://doi.org/10.1038/s41477-020-0655-x, 2020.

Friedl, M. A., Sulla-Menashe, D., Tan, B., Schneider, A., Ramankutty, N., Sibley, A., and Huang, X.: MODIS Collection 5 global land cover: Algorithm refinements and characterization of new datasets, Remote Sensing of Environment, 114, 168–182, https://doi.org/10.1016/j.rse.2009.08.016, 2010.

Friedlingstein, P., Meinshausen, M., Arora, V. K., Jones, C. D., Anav, A., Liddicoat, S. K., and Knutti, R.: Uncertainties in CMIP5 Climate Projections due to Carbon Cycle Feedbacks, Journal of Climate, 27, 511–526, https://doi.org/10.1175/JCLI-D-12-00579.1, 2014.

Friend, A. D., Stevens, A. K., Knox, R. G., and Cannell, M. G. R.: A process-based, terrestrial biosphere model of ecosystem dynamics (Hybrid v3.0), Ecological Modelling, 95, 249–287, https://doi.org/10.1016/S0304-3800(96)00034-8, 1997.

Friend, A. D., Arneth, A., Kiang, N. Y., Lomas, M., Ogee, J., Roedenbeckk, C., Running, S. W., Santaren, J.-D., Sitch, S., Viovy, N., Woodward, F. I., and Zaehle, S.: FLUXNET and modelling the global carbon cycle, Global Change Biology, 13, 610–633, https://doi.org/10.1111/j.1365-2486.2006.01223.x, 2007.

Garcia, E. S., Swann, A. L. S., Villegas, J. C., Breshears, D. D., Law, D. J., Saleska, S. R., and Stark, S. C.: Synergistic Ecoclimate Teleconnections from Forest Loss in Different Regions Structure Global Ecological Responses, PLoS One, 11, https://doi.org/10.1371/journal.pone.0165042, 2016.

Givnish, T.: Adaptive significance of evergreen vs. deciduous leaves: solving the triple paradox, Silva Fenn., 36, https://doi.org/10.14214/sf.535, 2002.

Gleason, K. E., Bradford, J. B., Bottero, A., D'Amato, A. W., Fraver, S., Palik, B. J., Battaglia, M. A., Iverson, L., Kenefic, L., and Kern, C. C.: Competition amplifies drought stress in forests across broad climatic and compositional gradients, Ecosphere, 8, e01849, https://doi.org/10.1002/ecs2.1849, 2017.

Green, J. K., Konings, A. G., Alemohammad, S. H., Berry, J., Entekhabi, D., Kolassa, J., Lee, J.-E., and Gentine, P.: Regionally strong feedbacks between the atmosphere and terrestrial biosphere, Nature Geosci, 10, 410–414, https://doi.org/10.1038/ngeo2957, 2017.

Hansen, J., Sato, M., Ruedy, R., Kharecha, P., Lacis, A., Miller, R., Nazarenko, L., Lo, K., Schmidt, G. A., Russell, G., Aleinov, I., Bauer, S., Baum, E., Cairns, B., Canuto, V., Chandler, M., Cheng, Y., Cohen, A., Del Genio, A., Faluvegi, G., Fleming, E., Friend, A., Hall, T., Jackman, C., Jonas, J., Kelley, M., Kiang, N. Y., Koch, D., Labow, G., Lerner, J., Menon, S., Novakov, T., Oinas, V., Perlwitz, Ja., Perlwitz, Ju., Rind, D., Romanou, A., Schmunk, R., Shindell, D., Stone, P., Sun, S., Streets, D., Tausnev, N., Thresher, D., Unger, N., Yao, M., and Zhang, S.: Climate simulations for 1880-2003 with GISS modelE, CLIMATE DYNAMICS, 29, 661–696, https://doi.org/10.1007/s00382-007-0255-8, 2007.

Harper, A. B., Williams, K. E., McGuire, P. C., Duran Rojas, M. C., Hemming, D., Verhoef, A., Huntingford, C., Rowland, L., Marthews, T., Breder Eller, C., Mathison, C., Nobrega, R. L. B., Gedney, N., Vidale, P. L., Otu-Larbi, F., Pandey, D., Garrigues, S., Wright, A., Slevin, D., De Kauwe, M. G., Blyth, E., Ardö, J., Black, A., Bonal, D., Buchmann, N., Burban, B., Fuchs, K., de Grandcourt, A., Mammarella, I., Merbold, L., Montagnani, L., Nouvellon, Y., Restrepo-Coupe, N., and Wohlfahrt, G.: Improvement of modeling plant responses to low soil moisture in JULESvn4.9 and evaluation against flux tower measurements, Geoscientific Model Development, 14, 3269–3294, https://doi.org/10.5194/gmd-14-3269-2021, 2021.

Harrison, S. P., Cramer, W., Franklin, O., Prentice, I. C., Wang, H., Brännström, Å., de Boer, H., Dieckmann, U., Joshi, J., Keenan, T. F., Lavergne, A., Manzoni, S., Mengoli, G., Morfopoulos, C., Peñuelas, J., Pietsch, S., Rebel, K. T., Ryu, Y., Smith, N. G., Stocker, B. D., and Wright, I. J.: Eco-evolutionary optimality as a means to improve vegetation and land-surface models, New Phytologist, 231, 2125–2141, https://doi.org/10.1111/nph.17558, 2021.

Hengeveld, G. M., Gunia, K., Didion, M., Zudin, S., Clerkx, A. P. P. M., and Schelhaas, M. J.: Global 1-degree Maps of Forest Area, Carbon Stocks, and Biomass, 1950-2010, , https://doi.org/10.3334/ORNLDAAC/1296, 2015.

Hikosaka, K. and Anten, N. P. R.: An evolutionary game of leaf dynamics and its consequences for canopy structure, Functional Ecology, 26, 1024–1032, https://doi.org/10.1111/j.1365-2435.2012.02042.x, 2012.

Hourdin, F., Mauritsen, T., Gettelman, A., Golaz, J.-C., Balaji, V., Duan, Q., Folini, D., Ji, D., Klocke, D., Qian, Y., Rauser, F., Rio, C., Tomassini, L., Watanabe, M., and Williamson, D.: The Art and Science of Climate Model Tuning, Bulletin of the American Meteorological Society, 98, 589–602, https://doi.org/10.1175/BAMS-D-15-00135.1, 2017.

Huang, M., Piao, S., Sun, Y., Ciais, P., Cheng, L., Mao, J., Poulter, B., Shi, X., Zeng, Z., and Wang, Y.: Change in terrestrial ecosystem water-use efficiency over the last three decades, GLOBAL CHANGE BIOLOGY, 21, 2366–2378, https://doi.org/10.1111/gcb.12873, 2015.

Huntzinger, D. N., Schwalm, C., Michalak, A. M., Schaefer, K., King, A. W., Wei, Y., Jacobson, A., Liu, S., Cook, R. B., Post, W. M., Berthier, G., Hayes, D., Huang, M., Ito, A., Lei, H., Lu, C., Mao, J., Peng, C. H., Peng, S., Poulter, B., Riccuito, D., Shi, X., Tian, H., Wang, W., Zeng, N., Zhao, F., and Zhu, Q.: The North American Carbon Program Multi-Scale Synthesis and Terrestrial Model Intercomparison Project – Part 1: Overview and experimental design,

1520 Geoscientific Model Development, 6, 2121–2133, https://doi.org/10.5194/gmd-6-2121-2013,
1521 2013.

1522 Ito, G., Romanou, A., Kiang, N. Y., Faluvegi, G., Aleinov, I., Ruedy, R., Russell, G., Lerner, P.,
1523 Kelley, M., and Lo, K.: Global Carbon Cycle and Climate Feedbacks in the NASA GISS
1524 ModelE2.1, Journal of Advances in Modeling Earth Systems, 12, e2019MS002030,
1525 https://doi.org/10.1029/2019MS002030, 2020.

1526 Jiang, L., Shi, Z., Xia, J., Liang, J., Lu, X., Wang, Y., and Luo, Y.: Transient Traceability
1527 Analysis of Land Carbon Storage Dynamics: Procedures and Its Application to Two Forest
1528 Ecosystems, Journal of Advances in Modeling Earth Systems, 9, 2822–2835,
1529 https://doi.org/10.1002/2017MS001004, 2017.

1530 Keenan, T. F., Hollinger, D. Y., Bohrer, G., Dragoni, D., Munger, J. W., Schmid, H. P., and
1531 Richardson, A. D.: Increase in forest water-use efficiency as atmospheric carbon dioxide
1532 concentrations rise, Nature, 499, 324–327, https://doi.org/10.1038/nature12291, 2013.

1533 Kelley, M., Schmidt, G. A., Nazarenko, L. S., Bauer, S. E., Ruedy, R., Russell, G. L., Ackerman,
1534 A. S., Aleinov, I., Bauer, M., Bleck, R., Canuto, V., Cesana, G., Cheng, Y., Clune, T. L., Cook,
1535 B. I., Cruz, C. A., Del Genio, A. D., Elsaesser, G. S., Faluvegi, G., Kiang, N. Y., Kim, D., Lacis,
1536 A. A., Leboissetier, A., LeGrande, A. N., Lo, K. K., Marshall, J., Matthews, E. E., McDermid,
1537 S., Mezuman, K., Miller, R. L., Murray, L. T., Oinas, V., Orbe, C., García-Pando, C. P.,
1538 Perlwitz, J. P., Puma, M. J., Rind, D., Romanou, A., Shindell, D. T., Sun, S., Tausnev, N.,
1539 Tsigaridis, K., Tselioudis, G., Weng, E., Wu, J., and Yao, M.-S.: GISS-E2.1: Configurations and
1540 Climatology, Journal of Advances in Modeling Earth Systems, 12, e2019MS002025,
1541 https://doi.org/10.1029/2019MS002025, 2020.

1542 Kim, Y., Moorcroft, P. R., Aleinov, I., Puma, M. J., and Kiang, N. Y.: Variability of phenology
1543 and fluxes of water and carbon with observed and simulated soil moisture in the Ent Terrestrial
1544 Biosphere Model (Ent TBM version 1.0.1.0.0), Geoscientific Model Development, 8, 3837–
1545 3865, https://doi.org/10.5194/gmd-8-3837-2015, 2015.

1546 Kyker-Snowman, E., Lombardozzi, D. L., Bonan, G. B., Cheng, S. J., Dukes, J. S., Frey, S. D.,
1547 Jacobs, E. M., McNellis, R., Rady, J. M., Smith, N. G., Thomas, R. Q., Wieder, W. R., and
1548 Grandy, A. S.: Increasing the spatial and temporal impact of ecological research: A roadmap for
1549 integrating a novel terrestrial process into an Earth system model, Global Change Biology, 28,
1550 665–684, https://doi.org/10.1111/gcb.15894, 2022.

1551 Levine, J. I., Levine, J. M., Gibbs, T., and Pacala, S. W.: Competition for water and species
1552 coexistence in phenologically structured annual plant communities, Ecology Letters, 25, 1110–
1553 1125, https://doi.org/10.1111/ele.13990, 2022.

1554 Litton, C. M., Raich, J. W., and Ryan, M. G.: Carbon allocation in forest ecosystems, Global
1555 Change Biol, 13, 2089–2109, https://doi.org/10.1111/j.1365-2486.2007.01420.x, 2007.

1556 Liu, H., Gleason, S. M., Hao, G., Hua, L., He, P., Goldstein, G., and Ye, Q.: Hydraulic traits are
1557 coordinated with maximum plant height at the global scale, Science Advances, 5, eaav1332,
1558 https://doi.org/10.1126/sciadv.aav1332, 2019.

Lloret, F., Escudero, A., Iriondo, J. M., Martínez-Vilalta, J., and Valladares, F.: Extreme climatic events and vegetation: the role of stabilizing processes, Global Change Biology, 18, 797–805, https://doi.org/10.1111/j.1365-2486.2011.02624.x, 2012.

Lu, R., Qiao, Y., Wang, J., Zhu, C., Cui, E., Xu, X., He, Y., Zhao, Z., Du, Y., Yan, L., Shen, G., Yang, Q., Wang, X., and Xia, J.: The U-shaped pattern of size-dependent mortality and its correlated factors in a subtropical monsoon evergreen forest, Journal of Ecology, 109, 2421–2433, https://doi.org/10.1111/1365-2745.13652, 2021.

Luo, Y.: Terrestrial carbon-cycle feedback to climate warming, ANNUAL REVIEW OF ECOLOGY EVOLUTION AND SYSTEMATICS, 38, 683–712, https://doi.org/10.1146/annurev.ecolsys.38.091206.095808, 2007.

Luo, Y. and Schuur, E. A. G.: Model parameterization to represent processes at unresolved scales and changing properties of evolving systems, Global Change Biology, 26, 1109–1117, https://doi.org/10.1111/gcb.14939, 2020.

Luo, Y., Weng, E., Wu, X., Gao, C., Zhou, X., and Zhang, L.: Parameter identifiability, constraint, and equifinality in data assimilation with ecosystem models, Ecological Applications, 19, 571–574, https://doi.org/10.1890/08-0561.1, 2009.

Luo, Y., Ogle, K., Tucker, C., Fei, S., Gao, C., LaDeau, S., Clark, J. S., and Schimel, D. S.: Ecological forecasting and data assimilation in a data-rich era, Ecological Applications, 21, 1429–1442, https://doi.org/10.1890/09-1275.1, 2011.

Luo, Y. Q., Randerson, J. T., Abramowitz, G., Bacour, C., Blyth, E., Carvalhais, N., Ciais, P., Dalmonech, D., Fisher, J. B., Fisher, R., Friedlingstein, P., Hibbard, K., Hoffman, F., Huntzinger, D., Jones, C. D., Koven, C., Lawrence, D., Li, D. J., Mahecha, M., Niu, S. L., Norby, R., Piao, S. L., Qi, X., Peylin, P., Prentice, I. C., Riley, W., Reichstein, M., Schwalm, C., Wang, Y. P., Xia, J. Y., Zaehle, S., and Zhou, X. H.: A framework for benchmarking land models, Biogeosciences, 9, 3857–3874, https://doi.org/10.5194/bg-9-3857-2012, 2012.

MacBean, N., Peylin, P., Chevallier, F., Scholze, M., and Schuermann, G.: Consistent assimilation of multiple data streams in a carbon cycle data assimilation system, Geoscientific Model Development, 9, 3569–3588, https://doi.org/10.5194/gmd-9-3569-2016, 2016.

Manzoni, S., Trofymow, J. A., Jackson, R. B., and Porporato, A.: Stoichiometric controls on carbon, nitrogen, and phosphorus dynamics in decomposing litter, Ecological Monographs, 80, 89–106, 2010.

Manzoni, S., Vico, G., Thompson, S., Beyer, F., and Weih, M.: Contrasting leaf phenological strategies optimize carbon gain under droughts of different duration, Advances in Water Resources, 84, 37–51, https://doi.org/10.1016/j.advwatres.2015.08.001, 2015.

McDowell, N. G.: Mechanisms Linking Drought, Hydraulics, Carbon Metabolism, and Vegetation Mortality, PLANT PHYSIOLOGY, 155, 1051–1059, https://doi.org/10.1104/pp.110.170704, 2011.

McDowell, N. G., Allen, C. D., Anderson-Teixeira, K., Aukema, B. H., Bond-Lamberty, B., Chini, L., Clark, J. S., Dietze, M., Grossiord, C., Hanbury-Brown, A., Hurtt, G. C., Jackson, R. B., Johnson, D. J., Kueppers, L., Lichstein, J. W., Ogle, K., Poulter, B., Pugh, T. A. M., Seidl, R., Turner, M. G., Uriarte, M., Walker, A. P., and Xu, C.: Pervasive shifts in forest dynamics in a changing world, Science, 368, https://doi.org/10.1126/science.aaz9463, 2020.

McNickle, G. G., Gonzalez-Meler, M. A., Lynch, D. J., Baltzer, J. L., and Brown, J. S.: The world's biomes and primary production as a triple tragedy of the commons foraging game played among plants, Proceedings of the Royal Society B: Biological Sciences, 283, 20161993, https://doi.org/10.1098/rspb.2016.1993, 2016.

Meir, P., Cox, P., and Grace, J.: The influence of terrestrial ecosystems on climate, Trends in Ecology & Evolution, 21, 254–260, https://doi.org/10.1016/j.tree.2006.03.005, 2006.

van der Molen, M. K., Dolman, A. J., Ciais, P., Eglin, T., Gobron, N., Law, B. E., Meir, P., Peters, W., Phillips, O. L., Reichstein, M., Chen, T., Dekker, S. C., Doubková, M., Friedl, M. A., Jung, M., van den Hurk, B. J. J. M., de Jeu, R. A. M., Kruijt, B., Ohta, T., Rebel, K. T., Plummer, S., Seneviratne, S. I., Sitch, S., Teuling, A. J., van der Werf, G. R., and Wang, G.: Drought and ecosystem carbon cycling, Agricultural and Forest Meteorology, 151, 765–773, https://doi.org/10.1016/j.agrformet.2011.01.018, 2011.

Montané, F., Fox, A. M., Arellano, A. F., MacBean, N., Alexander, M. R., Dye, A., Bishop, D. A., Trouet, V., Babst, F., Hessl, A. E., Pederson, N., Blanken, P. D., Bohrer, G., Gough, C. M., Litvak, M. E., Novick, K. A., Phillips, R. P., Wood, J. D., and Moore, D. J. P.: Evaluating the effect of alternative carbon allocation schemes in a land surface model (CLM4.5) on carbon fluxes, pools, and turnover in temperate forests, Geoscientific Model Development, 10, 3499–3517, https://doi.org/10.5194/gmd-10-3499-2017, 2017.

Niinemets, Ü. and Anten, N. P. R.: Packing the Photosynthetic Machinery: From Leaf to Canopy, in: Photosynthesis in silico: Understanding Complexity from Molecules to Ecosystems, edited by: Laisk, A., Nedbal, L., and Govindjee, Springer Netherlands, Dordrecht, 363–399, https://doi.org/10.1007/978-1-4020-9237-4_16, 2009.

Niinemets, Ü., Keenan, T. F., and Hallik, L.: A worldwide analysis of within-canopy variations in leaf structural, chemical and physiological traits across plant functional types, New Phytologist, 205, 973–993, https://doi.org/10.1111/nph.13096, 2015.

Niklas, K.: Plant Height and the Properties of Some Herbaceous Stems, Annals of Botany, 75, 133–142, https://doi.org/10.1006/anbo.1995.1004, 1995.

Nobre, C. A., Sellers, P. J., and Shukla, J.: Amazonian Deforestation and Regional Climate Change, J. Climate, 4, 957–988, https://doi.org/10.1175/1520-0442(1991)004<0957:ADARCC>2.0.CO;2, 1991.

Oliveira, R. S., Eller, C. B., Barros, F. de V., Hirota, M., Brum, M., and Bittencourt, P.: Linking plant hydraulics and the fast–slow continuum to understand resilience to drought in tropical ecosystems, New Phytologist, 230, 904–923, https://doi.org/10.1111/nph.17266, 2021.

Osnas, J. L. D., Lichstein, J. W., Reich, P. B., and Pacala, S. W.: Global Leaf Trait Relationships: Mass, Area, and the Leaf Economics Spectrum, Science, 340, 741–744, https://doi.org/10.1126/science.1231574, 2013.

Pan, Y., Birdsey, R. A., Phillips, O. L., and Jackson, R. B.: The Structure, Distribution, and Biomass of the World's Forests, Annual Review of Ecology, Evolution, and Systematics, 44, 593–622, https://doi.org/10.1146/annurev-ecolsys-110512-135914, 2013.

Park, H. and Jeong, S.: Leaf area index in Earth system models: how the key variable of vegetation seasonality works in climate projections, Environ. Res. Lett., 16, 034027, https://doi.org/10.1088/1748-9326/abe2cf, 2021.

Parton, W., Schimel, D., Cole, C., and Ojima, D.: Analysis of factors controlling soil organic matter levels in Great Plains grasslands, Soil Science Society of America Journal, 51, 1173–1179, https://doi.org/10.2136/sssaj1987.03615995005100050015x, 1987.

Parton, W. J., Stewart, J., and Cole, C.: DYNAMICS OF C, N, P AND S IN GRASSLAND SOILS - A MODEL, Biogeochemistry, 5, 109–131, https://doi.org/10.1007/BF02180320, 1988.

Pavlick, R., Drewry, D. T., Bohn, K., Reu, B., and Kleidon, A.: The Jena Diversity-Dynamic Global Vegetation Model (JeDi-DGVM): a diverse approach to representing terrestrial biogeography and biogeochemistry based on plant functional trade-offs, BIOGEOSCIENCES, 10, 4137–4177, https://doi.org/10.5194/bg-10-4137-2013, 2013.

Pielke, R. A., Sr, ., Avissar, RonI., Raupach, M., Dolman, A. J., Zeng, X., and Denning, A. S.: Interactions between the atmosphere and terrestrial ecosystems: influence on weather and climate, Global Change Biology, 4, 461–475, https://doi.org/10.1046/j.1365-2486.1998.t01-1-00176.x, 1998.

Potter, C., Klooster, S., Myneni, R., Genovese, V., Tan, P., and Kumar, V.: Continental-scale comparisons of terrestrial carbon sinks estimated from satellite data and ecosystem modeling 1982-1998, GLOBAL AND PLANETARY CHANGE, 39, 201–213, https://doi.org/10.1016/j.gloplacha.2003.07.001, 2003.

Potter, C. S., Randerson, J. T., Field, C. B., Matson, P. A., Vitousek, P. M., Mooney, H. A., and Klooster, S. A.: Terrestrial ecosystem production: A process model based on global satellite and surface data, Global Biogeochemical Cycles, 7, 811–841, https://doi.org/10.1029/93GB02725, 1993.

Powell, T. L., Galbraith, D. R., Christoffersen, B. O., Harper, A., Imbuzeiro, H. M. A., Rowland, L., Almeida, S., Brando, P. M., da Costa, A. C. L., Costa, M. H., Levine, N. M., Malhi, Y., Saleska, S. R., Sotta, E., Williams, M., Meir, P., and Moorcroft, P. R.: Confronting model predictions of carbon fluxes with measurements of Amazon forests subjected to experimental drought, New Phytologist, 200, 350–365, https://doi.org/10.1111/nph.12390, 2013.

Prentice, I. C., Cramer, W., Harrison, S. P., LEEMANS, R., Monserud, R. A., and Solomon, A. M.: A global biome model based on plant physiology and dominance, soil properties and climate, Journal of Biogeography, 19, 117–134, https://doi.org/10.2307/2845499, 1992.

1672 Prentice, I. C., Bondeau, A., Cramer, W., Harrison, S. P., Hickler, T., Lucht, W., Sitch, S., Smith,
1673 B., and Sykes, M. T.: Dynamic Global Vegetation Modeling: Quantifying Terrestrial Ecosystem
1674 Responses to Large-Scale Environmental Change, in: Terrestrial Ecosystems in a Changing
1675 World, edited by: Canadell, J. G., Pataki, D. E., and Pitelka, L. F., Springer Berlin Heidelberg,
1676 Berlin, Heidelberg, 175–192, https://doi.org/10.1007/978-3-540-32730-1_15, 2007.

1677 Prentice, I. C., Dong, N., Gleason, S. M., Maire, V., and Wright, I. J.: Balancing the costs of
1678 carbon gain and water transport: testing a new theoretical framework for plant functional
1679 ecology, Ecology Letters, 17, 82–91, https://doi.org/10.1111/ele.12211, 2014.

1680 Purves, D. and Pacala, S.: Predictive models of forest dynamics, SCIENCE, 320, 1452–1453,
1681 https://doi.org/10.1126/science.1155359, 2008.

1682 Purves, D. W., Lichstein, J. W., Strigul, N., and Pacala, S. W.: Predicting and understanding
1683 forest dynamics using a simple tractable model, PROCEEDINGS OF THE NATIONAL
1684 ACADEMY OF SCIENCES OF THE UNITED STATES OF AMERICA, 105, 17018–17022,
1685 https://doi.org/10.1073/pnas.0807754105, 2008.

1686 Randerson, J., Thompson, M., Conway, T., Fung, I., and Field, C.: The contribution of terrestrial
1687 sources and sinks to trends in the seasonal cycle of atmospheric carbon dioxide, Global
1688 Biogeochemical Cycles, 11, 535–560, https://doi.org/10.1029/97GB02268, 1997.

1689 Reich, P. B.: The world-wide 'fast–slow' plant economics spectrum: a traits manifesto, Journal
1690 of Ecology, 102, 275–301, https://doi.org/10.1111/1365-2745.12211, 2014.

1691 Reyer, C. P. O., Leuzinger, S., Rammig, A., Wolf, A., Bartholomeus, R. P., Bonfante, A., de
1692 Lorenzi, F., Dury, M., Gloning, P., Abou Jaoudé, R., Klein, T., Kuster, T. M., Martins, M.,
1693 Niedrist, G., Riccardi, M., Wohlfahrt, G., de Angelis, P., de Dato, G., François, L., Menzel, A.,
1694 and Pereira, M.: A plant's perspective of extremes: terrestrial plant responses to changing
1695 climatic variability, Global Change Biology, 19, 75–89, https://doi.org/10.1111/gcb.12023, 2013.

1696 Richardson, A. D., Anderson, R. S., Arain, M. A., Barr, A. G., Bohrer, G., Chen, G., Chen, J. M.,
1697 Ciais, P., Davis, K. J., Desai, A. R., Dietze, M. C., Dragoni, D., Garrity, S. R., Gough, C. M.,
1698 Grant, R., Hollinger, D. Y., Margolis, H. A., McCaughey, H., Migliavacca, M., Monson, R. K.,
1699 Munger, J. W., Poulter, B., Raczka, B. M., Ricciuto, D. M., Sahoo, A. K., Schaefer, K., Tian, H.,
1700 Vargas, R., Verbeeck, H., Xiao, J., and Xue, Y.: Terrestrial biosphere models need better
1701 representation of vegetation phenology: results from the North American Carbon Program Site
1702 Synthesis, GLOBAL CHANGE BIOLOGY, 18, 566–584, https://doi.org/10.1111/j.1365-
1703 2486.2011.02562.x, 2012.

1704 Rodriguez-Iturbe, I., Porporato, A., Ridolfi, L., Isham, V., and Coxi, D. R.: Probabilistic
1705 modelling of water balance at a point: the role of climate, soil and vegetation, Proceedings of the
1706 Royal Society of London. Series A: Mathematical, Physical and Engineering Sciences, 455,
1707 3789–3805, https://doi.org/10.1098/rspa.1999.0477, 1999.

1708 Rosenzweig, C. and Abramopoulos, F.: Land-Surface Model Development for the GISS GCM,
1709 Journal of Climate, 10, 2040–2054, https://doi.org/10.1175/1520-
1710 0442(1997)010<2040:LSMDFT>2.0.CO;2, 1997.

Scheiter, S., Langan, L., and Higgins, S. I.: Next-generation dynamic global vegetation models: learning from community ecology, New Phytologist, 198, 957–969, https://doi.org/10.1111/nph.12210, 2013.

Schmidt, G. A., Kelley, M., Nazarenko, L., Ruedy, R., Russell, G. L., Aleinov, I., Bauer, M., Bauer, S. E., Bhat, M. K., Bleck, R., Canuto, V., Chen, Y.-H., Cheng, Y., Clune, T. L., Del Genio, A., de Fainchtein, R., Faluvegi, G., Hansen, J. E., Healy, R. J., Kiang, N. Y., Koch, D., Lacis, A. A., LeGrande, A. N., Lerner, J., Lo, K. K., Matthews, E. E., Menon, S., Miller, R. L., Oinas, V., Oloso, A. O., Perlwitz, J. P., Puma, M. J., Putman, W. M., Rind, D., Romanou, A., Sato, M., Shindell, D. T., Sun, S., Syed, R. A., Tausnev, N., Tsigaridis, K., Unger, N., Voulgarakis, A., Yao, M.-S., and Zhang, J.: Configuration and assessment of the GISS ModelE2 contributions to the CMIP5 archive, Journal of Advances in Modeling Earth Systems, 6, 141–184, https://doi.org/10.1002/2013MS000265, 2014.

Sellers, P. J.: Modeling the Exchanges of Energy, Water, and Carbon Between Continents and the Atmosphere, Science, 275, 502–509, https://doi.org/10.1126/science.275.5299.502, 1997.

Sierra, C. A., Ceballos-Núñez, V., Metzler, H., and Müller, M.: Representing and Understanding the Carbon Cycle Using the Theory of Compartmental Dynamical Systems, Journal of Advances in Modeling Earth Systems, 10, 1729–1734, https://doi.org/10.1029/2018MS001360, 2018.

Simard, M., Pinto, N., Fisher, J. B., and Baccini, A.: Mapping forest canopy height globally with spaceborne lidar, Journal of Geophysical Research: Biogeosciences, 116, https://doi.org/10.1029/2011JG001708, 2011.

Singh, A. K., Dhanapal, S., and Yadav, B. S.: The dynamic responses of plant physiology and metabolism during environmental stress progression, Mol Biol Rep, 47, 1459–1470, https://doi.org/10.1007/s11033-019-05198-4, 2020.

Sitch, S., Smith, B., Prentice, I. C., Arneth, A., Bondeau, A., Cramer, W., Kaplan, J. O., Levis, S., Lucht, W., Sykes, M. T., Thonicke, K., and Venevsky, S.: Evaluation of ecosystem dynamics, plant geography and terrestrial carbon cycling in the LPJ dynamic global vegetation model, Global Change Biology, 9, 161–185, https://doi.org/10.1046/j.1365-2486.2003.00569.x, 2003.

Sitch, S., Friedlingstein, P., Gruber, N., Jones, S. D., Murray-Tortarolo, G., Ahlström, A., Doney, S. C., Graven, H., Heinze, C., Huntingford, C., Levis, S., Levy, P. E., Lomas, M., Poulter, B., Viovy, N., Zaehle, S., Zeng, N., Arneth, A., Bonan, G., Bopp, L., Canadell, J. G., Chevallier, F., Ciais, P., Ellis, R., Gloor, M., Peylin, P., Piao, S. L., Le Quéré, C., Smith, B., Zhu, Z., and Myneni, R.: Recent trends and drivers of regional sources and sinks of carbon dioxide, Biogeosciences, 12, 653–679, https://doi.org/10.5194/bg-12-653-2015, 2015.

Strigul, N., Pristinski, D., Purves, D., Dushoff, J., and Pacala, S.: Scaling from trees to forests: tractable macroscopic equations for forest dynamics, Ecological Monographs, 78, 523–545, https://doi.org/10.1890/08-0082.1, 2008.

Swenson, N. G. and Enquist, B. J.: Ecological and evolutionary determinants of a key plant functional trait: wood density and its community-wide variation across latitude and elevation, American Journal of Botany, 94, 451–459, https://doi.org/10.3732/ajb.94.3.451, 2007.

Swinehart, D. F.: The Beer-Lambert Law, J. Chem. Educ., 39, 333, https://doi.org/10.1021/ed039p333, 1962.

Tian, Y., Woodcock, C. E., Wang, Y., Privette, J. L., Shabanov, N. V., Zhou, L., Zhang, Y., Buermann, W., Dong, J., Veikkanen, B., Häme, T., Andersson, K., Ozdogan, M., Knyazikhin, Y., and Myneni, R. B.: Multiscale analysis and validation of the MODIS LAI product: I. Uncertainty assessment, Remote Sensing of Environment, 83, 414–430, https://doi.org/10.1016/S0034-4257(02)00047-0, 2002.

Tian, Y., Wang, Y., Zhang, Y., Knyazikhin, Y., Bogaert, J., and Myneni, R. B.: Radiative transfer based scaling of LAI retrievals from reflectance data of different resolutions, Remote Sensing of Environment, 84, 143–159, https://doi.org/10.1016/S0034-4257(02)00102-5, 2003.

Tifafi, M., Guenet, B., and Hatté, C.: Large Differences in Global and Regional Total Soil Carbon Stock Estimates Based on SoilGrids, HWSD, and NCSCD: Intercomparison and Evaluation Based on Field Data From USA, England, Wales, and France, Global Biogeochemical Cycles, 32, 42–56, https://doi.org/10.1002/2017GB005678, 2018.

Tilman, D.: Plant strategies and the dynamics and structure of plant communities, Princeton University Press, Princeton, N.J, 360 pp., 1988.

Verryckt, L. T., Vicca, S., Van Langenhove, L., Stahl, C., Asensio, D., Urbina, I., Ogaya, R., Llusià, J., Grau, O., Peguero, G., Gargallo-Garriga, A., Courtois, E. A., Margalef, O., Portillo-Estrada, M., Ciais, P., Obersteiner, M., Fuchslueger, L., Lugli, L. F., Fernandez-Garberí, P.-R., Vallicrosa, H., Verlinden, M., Ranits, C., Vermeir, P., Coste, S., Verbruggen, E., Bréchet, L., Sardans, J., Chave, J., Peñuelas, J., and Janssens, I. A.: Vertical profiles of leaf photosynthesis and leaf traits and soil nutrients in two tropical rainforests in French Guiana before and after a 3-year nitrogen and phosphorus addition experiment, Earth System Science Data, 14, 5–18, https://doi.org/10.5194/essd-14-5-2022, 2022.

Volaire, F.: A unified framework of plant adaptive strategies to drought: Crossing scales and disciplines, Global Change Biology, 24, 2929–2938, https://doi.org/10.1111/gcb.14062, 2018.

Wang, H., Prentice, I. C., Keenan, T. F., Davis, T. W., Wright, I. J., Cornwell, W. K., Evans, B. J., and Peng, C.: Towards a universal model for carbon dioxide uptake by plants, Nature Plants, 3, 734–741, https://doi.org/10.1038/s41477-017-0006-8, 2017.

Wang, Y.-P. and Goll, D. S.: Modelling of land nutrient cycles: recent progress and future development, Fac Rev, 10, 53, https://doi.org/10.12703/r/10-53, 2021.

Wang, Y.-P., Trudinger, C. M., and Enting, I. G.: A review of applications of model–data fusion to studies of terrestrial carbon fluxes at different scales, Agricultural and Forest Meteorology, 149, 1829–1842, https://doi.org/10.1016/j.agrformet.2009.07.009, 2009.

Wei, N., Xia, J., Zhou, J., Jiang, L., Cui, E., Ping, J., and Luo, Y.: Evolution of Uncertainty in Terrestrial Carbon Storage in Earth System Models from CMIP5 to CMIP6, Journal of Climate, 1, 1–33, https://doi.org/10.1175/JCLI-D-21-0763.1, 2022.

1787 Weiskopf, S. R., Myers, B. J. E., Arce-Plata, M. I., Blanchard, J. L., Ferrier, S., Fulton, E. A.,
1788 Harfoot, M., Isbell, F., Johnson, J. A., Mori, A. S., Weng, E., HarmáCˇková, Z. V., Londoño-
1789 Murcia, M. C., Miller, B. W., Pereira, L. M., and Rosa, I. M. D.: A Conceptual Framework to
1790 Integrate Biodiversity, Ecosystem Function, and Ecosystem Service Models, BioScience,
1791 biac074, https://doi.org/10.1093/biosci/biac074, 2022.

1792 Weng, E. and Luo, Y.: Relative information contributions of model vs. data to short- and long-
1793 term forecasts of forest carbon dynamics, ECOLOGICAL APPLICATIONS, 21, 1490–1505,
1794 2011.

1795 Weng, E., Luo, Y., Gao, C., and Oren, R.: Uncertainty analysis of forest carbon sink forecast
1796 with varying measurement errors: a data assimilation approach, Journal of Plant Ecology, 4,
1797 178–191, https://doi.org/10.1093/jpe/rtr018, 2011.

1798 Weng, E., Farrior, C. E., Dybzinski, R., and Pacala, S. W.: Predicting vegetation type through
1799 physiological and environmental interactions with leaf traits: evergreen and deciduous forests in
1800 an earth system modeling framework, Global Change Biology, 23, 2482–2498,
1801 https://doi.org/10.1111/gcb.13542, 2017.

1802 Weng, E., Dybzinski, R., Farrior, C. E., and Pacala, S. W.: Competition alters predicted forest
1803 carbon cycle responses to nitrogen availability and elevated CO2: simulations using an explicitly
1804 competitive, game-theoretic vegetation demographic model, Biogeosciences, 16, 4577–4599,
1805 https://doi.org/10.5194/bg-16-4577-2019, 2019.

1806 Weng, E. S., Malyshev, S., Lichstein, J. W., Farrior, C. E., Dybzinski, R., Zhang, T.,
1807 Shevliakova, E., and Pacala, S. W.: Scaling from individual trees to forests in an Earth system
1808 modeling framework using a mathematically tractable model of height-structured competition,
1809 Biogeosciences, 12, 2655–2694, https://doi.org/10.5194/bg-12-2655-2015, 2015.

1810 Wieder, W. R.: Regridded Harmonized World Soil Database v1.2, ,
1811 https://doi.org/10.3334/ORNLDAAC/1247, 2014.

1812 Wieder, W. R., Grandy, A. S., Kallenbach, C. M., and Bonan, G. B.: Integrating microbial
1813 physiology and physio-chemical principles in soils with the MIcrobial-MIneral Carbon
1814 Stabilization (MIMICS) model, BIOGEOSCIENCES, 11, 3899–3917,
1815 https://doi.org/10.5194/bg-11-3899-2014, 2014.

1816 Williams, M., Richardson, A. D., Reichstein, M., Stoy, P. C., Peylin, P., Verbeeck, H.,
1817 Carvalhais, N., Jung, M., Hollinger, D. Y., Kattge, J., Leuning, R., Luo, Y., Tomelleri, E.,
1818 Trudinger, C. M., and Wang, Y.-P.: Improving land surface models with FLUXNET data,
1819 Biogeosciences, 6, 1341–1359, https://doi.org/10.5194/bg-6-1341-2009, 2009.

1820 Woodward, F. I., Lomas, M. R., and Betts, R. A.: Vegetation-climate feedbacks in a greenhouse
1821 world, Phil. Trans. R. Soc. Lond. B, 353, 29–39, https://doi.org/10.1098/rstb.1998.0188, 1998.

1822 Xia, J., Luo, Y., Wang, Y.-P., and Hararuk, O.: Traceable components of terrestrial carbon
1823 storage capacity in biogeochemical models, Global Change Biology, 19, 2104–2116,
1824 https://doi.org/10.1111/gcb.12172, 2013.

Xia, J., Yuan, W., Wang, Y.-P., and Zhang, Q.: Adaptive Carbon Allocation by Plants Enhances the Terrestrial Carbon Sink, Sci Rep, 7, 3341, https://doi.org/10.1038/s41598-017-03574-3, 2017.

Xia, J., Yuan, W., Lienert, S., Joos, F., Ciais, P., Viovy, N., Wang, Y., Wang, X., Zhang, H., Chen, Y., and Tian, X.: Global Patterns in Net Primary Production Allocation Regulated by Environmental Conditions and Forest Stand Age: A Model-Data Comparison, Journal of Geophysical Research: Biogeosciences, 124, 2039–2059, https://doi.org/10.1029/2018JG004777, 2019.

Xu, T., White, L., Hui, D., and Luo, Y.: Probabilistic inversion of a terrestrial ecosystem model: Analysis of uncertainty in parameter estimation and model prediction, Global Biogeochemical Cycles, 20, GB2007, https://doi.org/10.1029/2005GB002468, 2006.

Yuan, W., Luo, Y., Liang, S., Yu, G., Niu, S., Stoy, P., Chen, J., Desai, A. R., Lindroth, A., Gough, C. M., Ceulemans, R., Arain, A., Bernhofer, C., Cook, B., Cook, D. R., Dragoni, D., Gielen, B., Janssens, I. A., Longdoz, B., Liu, H., Lund, M., Matteucci, G., Moors, E., Scott, R. L., Seufert, G., and Varner, R.: Thermal adaptation of net ecosystem exchange, Biogeosciences, 8, 1453–1463, https://doi.org/10.5194/bg-8-1453-2011, 2011.

Zeng, Z., Piao, S., Li, L. Z. X., Zhou, L., Ciais, P., Wang, T., Li, Y., Lian, X., Wood, E. F., Friedlingstein, P., Mao, J., Estes, L. D., Myneni, R. B., Peng, S., Shi, X., Seneviratne, S. I., and Wang, Y.: Climate mitigation from vegetation biophysical feedbacks during the past three decades, Nature Climate Change, 7, 432–436, https://doi.org/10.1038/nclimate3299, 2017.

Zhou, G., Houlton, B. Z., Wang, W., Huang, W., Xiao, Y., Zhang, Q., Liu, S., Cao, M., Wang, X., Wang, S., Zhang, Y., Yan, J., Liu, J., Tang, X., and Zhang, D.: Substantial reorganization of China's tropical and subtropical forests: based on the permanent plots, Global Change Biology, 20, 240–250, https://doi.org/10.1111/gcb.12385, 2014.

Zhou, J., Xia, J., Wei, N., Liu, Y., Bian, C., Bai, Y., and Luo, Y.: A traceability analysis system for model evaluation on land carbon dynamics: design and applications, Ecol Process, 10, 12, https://doi.org/10.1186/s13717-021-00281-w, 2021.

Zuleta, D., Arellano, G., Muller-Landau, H. C., McMahon, S. M., Aguilar, S., Bunyavejchewin, S., Cárdenas, D., Chang-Yang, C.-H., Duque, A., Mitre, D., Nasardin, M., Pérez, R., Sun, I.-F., Yao, T. L., and Davies, S. J.: Individual tree damage dominates mortality risk factors across six tropical forests, New Phytologist, 233, 705–721, https://doi.org/10.1111/nph.17832, 2022.

Page 30: [1] Deleted Weng, Ensheng (GISS-6110)[TRUSTEES OF COLUMBIA UNIVERSITY] 9/10/22 11:34:00 PM

Page 30: [1] Deleted Weng, Ensheng (GISS-6110)[TRUSTEES OF COLUMBIA UNIVERSITY] 9/10/22 11:34:00 PM

Page 30: [1] Deleted Weng, Ensheng (GISS-6110)[TRUSTEES OF COLUMBIA UNIVERSITY] 9/10/22 11:34:00 PM

Page 30: [1] Deleted Weng, Ensheng (GISS-6110)[TRUSTEES OF COLUMBIA UNIVERSITY] 9/10/22 11:34:00 PM

Page 42: [2] Deleted Weng, Ensheng (GISS-6110)[TRUSTEES OF COLUMBIA UNIVERSITY] 9/8/22 4:07:00 PM